



[Keldysh Institute](#) • [Publication search](#)

[Keldysh Institute preprints](#) • [Preprint No. 8, 2008](#)



**T. Beuselinck, C. Van Bavinchove,  
[Sazonov V.V.](#), [Chebukov S.Yu.](#)**

Analysis of Quasi-steady  
Component in Acceleration  
Measurement Data Obtained  
Onboard Foton M-2

***Recommended form of bibliographic references:*** T. Beuselinck, C. Van Bavinchove, Sazonov V.V., Chebukov S.Yu. Analysis of Quasi-steady Component in Acceleration Measurement Data Obtained Onboard Foton M-2. Keldysh Institute preprints, 2008, No. 8, 38 p. URL: <http://library.keldysh.ru/preprint.asp?id=2008-8&lg=e>

RUSSIAN ACADEMY OF SCIENCES  
KELDYSH INSTITUTE OF APPLIED MATHEMATICS

T. Beuselinck, C. Van Bavinchove, V.V. Sazonov, S.Yu. Chebukov

**ANALYSIS OF QUASI-STEADY COPONENT IN ACCELERATION  
MEASUREMENT DATA OBTAINED ONBOARD *FOTON M-2***

Moscow – 2008

## Abstract

The paper presents the results of the investigation of the measurement data obtained onboard the spacecraft *Foton M-2* by the triaxial accelerometer TAS3. TAS3 had a sample rate equal to 1000 readings per second and produced the data in a wide spectral range. We extracted the low-frequency component from those data and compared it with its calculation analog that was obtained by reconstruction of the spacecraft attitude motion. The spectral analysis of functions presenting the both results was done. It confirmed the influence of the Earth magnetic field upon the measurement data. When we made a correction for this influence and refined the position of the accelerometer onboard the spacecraft the results obtained in these both ways, coincided with each other very exactly (the mean-root-square error doesn't exceed  $10^{-6}$  m/s<sup>2</sup>).

**Т. Бойзелинк, К. Ван Бавинхов, В.В. Сазонов, С.Ю. Чебуков. Анализ низкочастотной составляющей в измерениях микроускорения, выполненных на спутнике *Фотон М-2*.** Исследована низкочастотная составляющая в данных измерений микроускорения, выполненных на спутнике Фотон М-2 трехкомпонентным акселерометром TAS-3. Эти данные получены со скоростью выборки 1000 отсчетов в секунду и имеют широкий частотный диапазон. Низкочастотная составляющая выделялась из них с помощью дискретных рядов Фурье. Исследование состояло в сравнении этой составляющей с ее расчетным аналогом, найденным по реконструкции вращательного движения спутника. Посредством спектрального анализа функций, представляющих результаты определения низкочастотного микроускорения обоими методами, установлено влияние магнитного поля Земли на показания акселерометра. После внесения поправки за такое влияние результаты, полученные этими двумя способами совпали со среднеквадратической ошибкой менее  $10^{-6}$  м/с<sup>2</sup>.

**1. Two ways of determining quasi-steady residual accelerations onboard a spacecraft.** This paper contains the analysis of the measurement data obtained onboard the spacecraft *Foton M-2* by the triaxial accelerometer TAS3. The spacecraft was a free flyer. It was in orbit during the period 31.05.2005 – 16.06.2005. The accelerometer was produced by the company RedShift Design and Engineering BVBA (Sint Niklaas, Belgium). It was placed on the furnace *Polizon* and operated continuously during almost the whole flight. Its measurements served for monitoring of microgravity environment during technological experiments.

The residual accelerations onboard a free flyer can be decomposed into two components, vibration (high-frequency) and quasi-steady (low-frequency) ones. Usually, the spectrum of a vibration component contains frequencies from above a few hundredths of Hz. A quasi-steady component has the spectrum in the range from zero to a few thousandths of Hz. We analyze below only a quasi-steady acceleration component. The following reasons cause it: a spacecraft attitude motion, a gradient of the Earth gravitational field, and an atmosphere drag.

That component can be found by two ways. The first way consists in a low-frequency filtration of measurement data of an onboard accelerometer. This way makes high demands for sensitivity and stability of the accelerometer in a low-frequency range. Besides, this way gives the quasi-steady acceleration component only at the point of the accelerometer location. The second way is based on a reconstruction of a satellite real attitude motion and a subsequent calculation of the acceleration along the reconstructed motion by the well-known formula. Let us remind that formula and some related definitions.

Let a spacecraft be a rigid body and a point  $P$  be fixed with its frame. The difference between the gravitational field strength at the point  $P$  and the absolute acceleration of that point is called a residual acceleration at the point  $P$ . We denote the difference by  $\mathbf{b}$ . This quantity plays a part of  $\mathbf{g}$  in orbital experiments. We assume the atmosphere drag is a sole nongravitational influence upon the spacecraft. Then  $\mathbf{b}$  is defined by the formula [1]

$$\mathbf{b} = \mathbf{r} \times \dot{\boldsymbol{\omega}} + \boldsymbol{\omega} \times (\mathbf{r} \times \boldsymbol{\omega}) + \frac{\mu_e}{|\mathbf{R}|^3} \left[ \frac{3(\mathbf{R} \cdot \mathbf{r})\mathbf{R}}{|\mathbf{R}|^2} - \mathbf{r} \right] + c\rho_a |\mathbf{v}| \mathbf{v}. \quad (1)$$

Here,  $\mathbf{r} = \overrightarrow{OP}$ , the point  $O$  is the spacecraft mass center,  $\boldsymbol{\omega}$  is the absolute angular rate of the spacecraft, the dot above a letter denotes differentiation with respect to time  $t$ ,  $\mu_e$  is the gravitational parameter of the Earth,  $\mathbf{R}$  is the geocentric radius vector of the point  $O$ ,  $\mathbf{v}$  is the velocity of the point  $O$  with respect to the Earth surface,  $\rho_a$  is the atmosphere density at that point,  $c$  is the spacecraft ballistic coefficient.

The reconstruction of the spacecraft attitude motion can be made by processing measurement data of onboard sensors. We can do with indirect measurements if we reconstruct a spacecraft attitude motion using a full system of motion equations of a rigid body. In particular, we reconstructed the motion of *Foton-12* and *Foton M-2* based on measurements of triaxial magnetometers [2, 3]. The measurement data were accumulated continually during the most part of the flight

but the procedure deals with data segments of a few hours length. The measurement data on each such segment are processed jointly using the least squares method and integration of the spacecraft attitude motion equations. The procedure results in the solution of those equations that approximates measurements. Then, we calculate the acceleration at a prescribed point of the spacecraft as a function of time along the found solution by formula (1). This formula was derived for a general situation without any frequency restrictions. But it gives just a quasi-steady acceleration component in *Foton*'s case [4].

The second way is rather universal. It allows determining the quasi-steady acceleration component at any point fixed with the spacecraft body but it does not take into account possible local acceleration features. We can follow various reasons when choice the point  $P$  for application of formula (1) but one reason has to be picked out especially. We must consider as  $P$  the points, where accelerometers were placed. Then we can compare results obtained in both discussed ways. It allows us to check the accelerometers and the calculation model.

Such a comparison is made below for the accelerometer TAS3 located on-board *Foton M-2*. The results, obtained in these both ways, coincided with each other very exactly after we refined the accelerometer position and corrected the filtered data for the influence of the Earth magnetic field. This influence was revealed by spectral analysis of the filtered and calculated data as well as the Earth magnetic field strength in the spacecraft fixed coordinate system.

**2. Calculation of quasi-steady accelerations by reconstruction of spacecraft attitude motion.** The method of the reconstruction consists in following [3]. We assign a time interval  $t_0 \leq t \leq t_1$  and, using the measurement data, construct on it the functions  $\hat{h}_i(t)$  ( $i=1, 2, 3$ ) approximating the components of the strength of the local magnetic field in the spacecraft structural coordinate system  $y_1y_2y_3$ . The axis  $y_1$  is the longitudinal axis of the spacecraft and is directed from the landing capsule to the device unit. We suppose that the local magnetic field coincide with the Earth one at the point  $O$  and calculate its components  $H_i(t)$  ( $i=1, 2, 3$ ) in the Greenwich coordinate system  $Y_1Y_2Y_3$  along the spacecraft orbit basing on the analytical model IGRF2005. Certain relations should link two sets of functions obtained. The condition of the closest fit of these relations on the interval  $t_0 \leq t \leq t_1$  defines the solution to the spacecraft attitude motion equations that approximates the real motion.

The gravitational and some other torques are taken into account in those equations. The equations are written in the coordinate system  $x_1x_2x_3$  formed by the principal central axes of inertia of the spacecraft. The angles between the axes  $x_i$  and  $y_i$  did not exceed several degrees. Denote by  $\|g_{ij}\|_{i,j=1}^3$  the matrix of transition from the system  $x_1x_2x_3$  to the system  $Y_1Y_2Y_3$ , where  $g_{ij}$  was the cosine of the angle between axes  $Y_i$  and  $x_j$ . The phase vector of the attitude motion equations consists of the quantities  $g_{1i}$ ,  $g_{2i}$ , and the components  $\omega_i$  of the spacecraft angu-

lar rate  $\omega$  in the system  $x_1x_2x_3$  ( $i=1, 2, 3$ ). The quantities  $g_{3i}$  are calculated by formulas  $g_{31} = g_{12}g_{23} - g_{13}g_{22}$ , etc. The matrix of transition from the system  $x_1x_2x_3$  to the structural coordinate system is denoted by  $\|b_{ij}\|_{i,j=1}^3$ . Here,  $b_{ij}$  is the cosine of the angle between axes  $y_i$  and  $x_j$ . We consider the solution to the motion equations minimizing the functional

$$\Phi = \sum_{n=0}^N \sum_{i=1}^3 [\hat{h}_i(t_0 + n\tau) - \Delta_i - h_i(t_0 + n\tau)]^2, \quad (2)$$

$$h_i(t) = \sum_{j,k=1}^3 H_j(t) g_{jk}(t) b_{ik}, \quad \tau = \frac{t_1 - t_0}{N}$$

as an approximation of the real attitude motion of the spacecraft on the interval  $t_0 \leq t \leq t_1$ . Here,  $\Delta_i$  are constant shifts in the measurement data. Functional (2) is minimized on the initial conditions of the solution at the point  $t_0$  and parameters of the mathematical model. The latter include the parameters of the motion equations, the shifts  $\Delta_i$ , and three angles specifying the transition matrix  $\|b_{ij}\|$ . Usually, we take  $t_1 - t_0 \approx 100 \div 300$  min and  $\tau \approx 1$  min.

The example of reconstructing the attitude motion of the spacecraft is presented in Fig. 1. This figure consists of two parts. Fig. 1a illustrates the agreement of the functions  $\hat{h}_i(t)$  and  $H_i(t)$  by the found spacecraft motion. Here, the solid lines present the plots of the functions  $h_i(t)$  defined in (2); the marks indicate the points  $(t_0 + n\tau, \hat{h}_i(t_0 + n\tau) - \Delta_i)$ ,  $n=0, 1, \dots, N$ . The quality of the agreement is characterized by the standard deviation  $\sigma \approx \sqrt{\Phi_{\min}/3N}$ , where  $\Phi_{\min}$  is the minimum value of functional (2). We have  $\sigma = 1147 \gamma$  in this example.

Fig. 1b presents the plots of the angular rate components  $\omega_i(t)$ . One can see from the plots that the spacecraft motion was similar to Euler's regular precession of an axisymmetric rigid body with the symmetry axis  $x_1$ . *Foton M-2* was not exactly axisymmetric but it had close inertia moments regarding to the axes  $x_2$  and  $x_3$ . One can also treat that motion as the motion near the stationary rotation of a triaxial rigid body around its principal central axis of the minimal inertia moment. In this motion

$$\omega_1 = \Omega, \quad \omega_2 = W \sin(p\Omega t + \alpha), \quad \omega_3 = Wr \cos(p\Omega t + \alpha), \quad (3)$$

$$p = \sqrt{\frac{(I_2 - I_1)(I_3 - I_1)}{I_2 I_3}}, \quad r = \sqrt{\frac{I_2(I_2 - I_1)}{I_3(I_3 - I_1)}}.$$

Here,  $\alpha$ ,  $\Omega$ , and  $W$  are arbitrary constants,  $0 \ll W \ll |\Omega|$ ,  $I_i$  ( $i=1, 2, 3$ ) are the moments of inertia of the spacecraft with respect to the axes  $x_i$ , i.e. its principal central moments of inertia. *Foton M-2* had  $p = 0.734$ ,  $r = 1.032$ ; the constants  $\Omega$ , and  $W$  for each processed interval  $[t_0, t_1]$  are evaluated as

$$\Omega = \frac{1}{t_1 - t_0} \int_{t_0}^{t_1} \omega_1 dt, \quad W = \frac{1}{t_1 - t_0} \int_{t_0}^{t_1} \sqrt{\omega_2^2 + r^{-2} \omega_3^2} dt.$$

The accuracy of formulas (3) is characterized by the quantities

$$\delta\Omega = \left[ \frac{1}{t_1 - t_0} \int_{t_0}^{t_1} (\omega_1 - \Omega)^2 dt \right]^{1/2}, \quad \delta W = \left[ \frac{1}{t_1 - t_0} \int_{t_0}^{t_1} (\sqrt{\omega_2^2 + r^{-2} \omega_3^2} - W)^2 dt \right]^{1/2}.$$

The motion in Fig. 1 is characterized by the values  $\Omega = 1.149$  deg./s,  $\delta\Omega = 0.0021$  deg./s,  $W = 0.112$  deg./s, and  $\delta W = 0.0103$  deg./s.

Fig. 1 illustrates the satellite motion in the last hours of the magnetic field measurements. The satellite motion was reconstructed in the same manner for preceding days too [3]. Table 1 presents some results obtained in 13 time intervals. Each interval has the length of 270 min. The table contains their initial points  $t_0$  (the date and time) and the respective values of  $\sigma$ ,  $\Omega$ ,  $\delta\Omega$ ,  $W$ , and  $\delta W$ . Fig. 1 corresponds to interval 13.

Table 1. Basic results of processing the *Mirage* measurements

Inter- val	Date 05/06.2005	$t_0$ UTC	$\sigma, \gamma$	$\Omega,$ deg./s	$\delta\Omega,$ deg./s	$W,$ deg./s	$\delta W,$ deg./s
1	31	23:25:30	2947	0.200	0.017	0.107	0.045
2	1	11:11:08	1318	0.312	0.014	0.082	0.045
3	2	00:11:50	1428	0.441	0.013	0.099	0.038
4	2	11:12:25	1566	0.521	0.012	0.066	0.029
5	3	00:13:07	1038	0.645	0.016	0.070	0.024
6	3	11:13:43	1231	0.745	0.0070	0.056	0.016
7	4	00:14:24	1381	0.789	0.0059	0.094	0.029
8	4	13:15:06	1111	0.849	0.0067	0.145	0.013
9	5	10:36:15	1340	0.931	0.0059	0.147	0.011
10	6	11:17:34	1094	1.008	0.0072	0.146	0.011
11	7	09:18:45	1136	1.066	0.0039	0.131	0.0099
12	8	09:20:02	1210	1.111	0.0058	0.114	0.010
13	9	09:21:20	1147	1.149	0.0021	0.112	0.010

The table shows that the angular rate of the satellite increased and formulas (3) became more precise coupled with this increase (note the behavior of  $\delta\Omega$  and  $\delta W$ ). The final mode of the attitude motion was formed a few days before the flight termination. There were  $\Omega = 1.3$  deg./s and  $W = 0.1$  deg./s [5].

Fig. 2a illustrates the residual acceleration calculated by formula (1) for the motion in Fig. 1. Calculations were made for the point  $P$  with  $\mathbf{r} = (-0.06 \text{ m}, 0, -0.29 \text{ m})$ , where the sensors of the accelerometer TAS3 should be

located. The plots in the figure represent time the components of the vector  $\mathbf{b} = (b_1, b_2, b_3)$  as functions of time. Here and below, components of vectors are referred to the structural coordinate system. Calculating the last term in formula (1), we used the ballistic coefficient obtained by processing trajectory measurements [3]. The atmosphere density in (1) was calculated according to GOST R (state standard) 25645.166-2004 – Model of the upper atmosphere for ballistic calculations. The matrices  $\|b_{ij}\|$  of different intervals  $[t_0, t_1]$  somewhat differed from each other. The acceleration was calculated in each interval  $t_0 \leq t \leq t_1$  using the matrix  $\|b_{ij}\|$  obtained just for this interval.

**3. Filtration of low-frequency component from TAS3 data.** The accelerometer TAS3 measured an apparent acceleration  $(-\mathbf{b})$ . Its sensitive axes were parallel to the axes of structural coordinate system but axes, corresponding to  $y_1$  and  $y_3$ , had opposite directions. TAS3 had a sample rate equal to 1000 readings per second and produced the data in a wide spectral range. The low-frequency filtration of the data was made using finite Fourier series independently for each vector component.

Let  $M$  and  $N$  be natural numbers,  $z_i$  ( $i = 1, 2, \dots, MN$ ) be a segment of the scalar measurement data. We refer the measurement  $z_i$  to the instant  $t_i = ih$ ,  $h > 0$ , and seek the low-frequency component, contained in these data, in the form

$$z(t) = a_N + a_{N+1}t + \sum_{n=1}^{N-1} a_n \sin \frac{\pi n t}{NMh}. \quad (4)$$

Here,  $a_n$  are coefficients. They are found by the least squares method. The simple explicit formulas are available to calculate them [1]. Some oscillations with relatively high frequencies are often revealed in function (4) that was obtained in this way. In order to remove them, some terms in (4) are modified using the correctional multipliers

$$a_n \frac{N-n}{N-N_1} \rightarrow a_n \quad (n = N_1 + 1, N_1 + 2, \dots, N-1).$$

Here,  $N_1$  is the integer part of the number  $N/2$ . As a rule, we don't use expressions (4) directly but deal with their values

$$\tilde{z}_n = z(\tilde{t}_n), \quad \tilde{t}_n = n\tilde{h} \quad (n = 0, 1, \dots, N), \quad \tilde{h} = Mh. \quad (5)$$

We refer to these values as the filtered data. We denote the vector components of the filtered acceleration data by  $b'_i$  ( $i = 1, 2, 3$ ).

In all examples below, expressions (4) were constructed using data segments with a length of 270 min. They were certain of the segments listed in Table 1. The above procedure was applied at  $h = 0.001$  s,  $M = 30000$ , and  $N = 540$ . The spectrum of functions, obtained in this way, locates within the limits from 0 to 0.017 Hz. TAS3 measurements have erroneous constant biases in each vector component. We changed on that reason the coefficient  $a_N$  in (4) to obtain zero mean value of data (5). Fig. 3a presents the example of the filtered data from TAS3 measurements. It illustrates the same time interval as Fig. 2a. Each coordinate system

in Fig. 3a contains a couple of plots. The plot of expression (4) has greater oscillations.

TAS3 measurements contain not only erroneous constant biases but an erroneous infra low-frequency component too. Such a component has frequencies less than 0.00005 Hz. It is lacking in calculated accelerations. One should guess it by comparing the plots in Fig. 3a with the respective plots in Figs. 2a. This effect takes place for the other intervals of Table 1. To obtain the likeness between the filtered low-frequency component in TAS3 data and its calculated analog, we eliminated the infra low-frequency component from data (5). First, we smoothed these data by the expression

$$Z(t) = A_{K+1} + A_{K+2}t + \sum_{k=1}^K A_k \sin \frac{\pi kt}{N\tilde{h}},$$

where the coefficients  $A_k$  were found by the least squares method. We took  $K = 10$  in the case of  $N = 540$ . The function  $Z(t)$  represented the sought ultra low-frequency component. Then we replaced the quantities  $\tilde{z}_n = z(\tilde{t}_n)$  in (5) by the quantities  $\tilde{z}_n = z(\tilde{t}_n) - Z(\tilde{t}_n)$ . Just new data (5) are referred bellow as filtered ones. These new data are again the values of certain new expression (4).

Fig. 3b presents the plots of the functions  $z(t) - Z(t)$  related to interval 13. Fluent curves in Fig. 3a present the plots of the functions  $Z(t)$ . When  $N = 540$  and  $K = 10$ , the described method of filtering does not change the amplitudes of harmonic components in the measurement data with frequencies from  $3.0 \cdot 10^{-4}$  to  $8.3 \cdot 10^{-3}$  Hz; the filtered data don't contain harmonics with frequencies higher than  $16.7 \cdot 10^{-3}$  Hz and lower than  $1.5 \cdot 10^{-4}$  Hz.

Fig. 2b gives a comparison of low-frequency component in TAS3 data on interval 13 with its calculated analog. The plots, drawn by fine lines, were drawn using the filtered data; the plots, drawn by thick lines, repeat corresponding plots in Fig. 2a. The thick lines were obtained from the respective lines in Fig. 3b by the following way. First, we changed the sign of the function  $b'_2(t)$  (thereby, we made the transform  $-\mathbf{b} \rightarrow \mathbf{b}$ ). Then, we added the constant biases to the functions  $b'_i(t)$  to obtain the equalities  $\langle b'_i(t) \rangle = \langle b_i(t) \rangle$  ( $i = 1, 2, 3$ ). The operator of mean value  $\langle \dots \rangle$  was defined above.

Fig. 2b shows the functions  $b_1(t)$  and  $b'_1(t)$  are close. This fact is valid for intervals 7 – 13 in Table 1. The oscillations of  $b_1$  and  $b'_1$  in them have large amplitudes and frequencies increasing coupled with  $\Omega$ . It is difficult to see proximity in the case of functions  $b_2(t)$ ,  $b'_2(t)$  or  $b_3(t)$ ,  $b'_3(t)$ . This is valid for all intervals in Table 1. C. Van Bavinchove, one of TAS3 creators, supposed the discrepancy was caused of the Earth magnetic field influence. The next sections contain the analysis confirming this hypothesis.

**4. Spectral analysis of low-frequency acceleration component.** Judging from the plots in Figs. 2 and 3, the low-frequency component of the acceleration onboard *Foton M-2* can be represented as a linear combination of a few harmonics

(cyclic trends) with frequencies that are incommensurable in the general case. The representation promises to be especially exact in intervals 7 – 13 in Table 1. Searching for such harmonics is a typical problem of the time series analysis [8, 9]. In our case this problem was solved as follows.

Let data (5) be the filtered data of an acceleration vector component. Expression (4) that generated them contains harmonics with a fixed set of frequencies. This set has a formal sense and does not reflect itself spectral properties of the data. In order to reveal these properties let us try to fit data (5) by the function

$$z_{\text{ap}}(t) = a_0 + a \cos 2\pi ft + b \sin 2\pi ft \quad (f > 0), \quad (6)$$

where  $a_0$ ,  $a$ ,  $b$ , and  $f$  are parameters. We will seek the values of these parameters by the least squares method. We make up the following expression

$$\Psi = \sum_{n=0}^N [\tilde{z}_n - z_{\text{ap}}(\tilde{t}_n)]^2 \quad (7)$$

and minimize it over  $a_0$ ,  $a$ ,  $b$ , and  $f$ . The function  $\Psi = \Psi(a_0, a, b, f)$  has a lot of local minima and only part of them corresponds to real harmonics. To find such minima, we solve a number of identical linear least squares problems and calculate the function

$$\Psi_1(f) = \min_{a_0, b, c} \Psi(a_0, b, c, f)$$

at points of a sufficiently fine uniform grid on the interval  $0 \leq f \leq 1/(2\tilde{h})$ . Then the plot of this function is drawn and the approximate values of minimum points are found. The abscissas of significant (in the value of  $\Psi_1$ ) minima are the frequencies of desired harmonics. Let the frequencies  $f_k^\circ$  ( $k = 1, 2, \dots, M$ ;  $M \ll N$ ) be found in this way. We seek the trend corresponding to them in the form

$$x_{\text{ap}}(t) = a_0 + \sum_{k=1}^M (a_k \cos 2\pi f_k t + b_k \sin 2\pi f_k t), \quad (8)$$

where  $a_0$ ,  $a_k$ ,  $b_k$ , and  $f_k \approx f_k^\circ$  ( $k = 1, 2, \dots, M$ ) are parameters. The values of these parameters are found by minimization of the function specified by relations (7) and (8) using Gauss-Newton's method. This least squares problem is nonlinear. The initial approximation to its solution is formed by the frequencies  $f_k^\circ$  and the solution of the linear least squares problem (7), (8) over  $a_0$ ,  $a_k$ ,  $b_k$  with these frequencies.

In order to verify the found solution by simple means, we considered so-called Schuster's periodogram [6, 7]

$$I(f) = \left[ \sum_{n=0}^N (\tilde{z}_n - \bar{z}) \cos 2\pi f n \tilde{h} \right]^2 + \left[ \sum_{n=0}^N (\tilde{z}_n - \bar{z}) \sin 2\pi f n \tilde{h} \right]^2, \quad \bar{z} = \frac{1}{N+1} \sum_{n=0}^N \tilde{z}_n$$

along with the function  $\Psi_1(f)$ . Let data (5) under study be generated by function (8), where  $N \gg M$ . Then  $a_0 \approx \bar{z}$ , the periodogram has local maxima at points

$f \approx f_k$ , while  $a_k^2 + b_k^2 \approx 4I(f_k)(N+1)^{-2}$  ( $k = 1, 2, \dots, M$ ). Thus, studying the periodogram maxima one can evaluate the frequencies and amplitudes of harmonic components in data (5).

We present below the plots of the functions

$$E(f) = \sqrt{\frac{\Psi_1(f)}{N-2}}, \quad A(f) = \frac{2}{N+1} \sqrt{I(f)}$$

instead of functions  $\Psi_1(f)$  and  $I(f)$ . The minima of the function  $E(f)$  expresses the root mean square error of approximation of data (5) by sole cyclic trend (6), while the maxima of function  $A(f)$  estimate the amplitude  $\sqrt{a^2 + b^2}$ .

Consider as an example the results of spectral analysis of the acceleration in Fig. 3b. The plots of the functions  $E(f)$  and  $A(f)$  for the acceleration components  $b'_1$  and  $b'_2$  are shown in Figs. 4a, 5a. The component  $b'_3$  has essentially the same frequency properties as  $b'_2$  and so it is not considered in detail. The minimum points of the functions  $A(f)$  differ from the maximum points of the respective functions  $E(f)$  no more than  $5 \cdot 10^{-6}$  Hz.

Each function  $b'_1(t)$  or  $b'_2(t)$  contains several harmonics. Constructing appropriate expressions (8), we take into account all clear-cut harmonics (corresponding to well pronounced extrema of  $E(f)$  and  $A(f)$ ) and some of slightly definite ones. To analyze these expressions, we introduce the following designations. We denote by  $b'_{i,\text{ap}}(t)$  expression (8) approximated the function  $b'_i(t)$  ( $i = 1, 2, 3$ ). Plots of the functions  $\Delta b'_i(t) = b'_i(t) - b'_{i,\text{ap}}(t)$  serve to check the approximation. We refer to the quantity  $A_k = \sqrt{a_k^2 + b_k^2}$  as the amplitude of a harmonic with the frequency  $f_k$  in (8). The frequencies and amplitudes of harmonics of  $b'_{i,\text{ap}}(t)$  are denoted as  $f_k^{(i)}$  and  $A_k^{(i)}$ . We also use analogous designations in the case of functions  $b_i(t)$  and  $h_i(t)$  defined in Section 2. We take  $10^{-3}$  Hz and  $10^{-6}$  m/s<sup>2</sup> as the units for frequencies and acceleration amplitudes respectively.

The plots of functions  $b'_i(t)$ ,  $b'_{i,\text{ap}}(t)$ , and  $\Delta b'_i(t)$  ( $i = 1, 2$ ) are given in Figs. 4b, 5b. We see the approximation is sufficiently exact. This fact confirms the accuracy of finding the frequencies  $f_k^{(i)}$  and amplitudes  $A_k^{(i)}$  that are listed in Table 2. Here, the frequencies with identical subscripts are approximately equal and empty cells mean that corresponding harmonics are absent in a respective function.

Following the least squares method, we estimate the accuracy of determination of the quantities  $f_k^{(i)}$  and  $A_k^{(i)}$  by corresponding standard deviations. These standard deviations seem to be not adequate from the probabilistic point of view in this situation but they give useful information. The frequency  $f_8^{(1)}$  has the least standard deviation equal to 0.00021; standard deviations of the frequencies  $f_{11}^{(2,3)}$  and  $f_{13}^{(2,3)}$  don't exceed 0.001; standard deviations of the other frequencies are

within the limits  $0.001 \div 0.005$ . Standard deviations of the amplitudes  $A_k^{(1)}$  and  $A_k^{(2,3)}$  don't exceed 0.3 and 0.15 correspondingly.

The standard deviations of the frequencies look too small. We point out for comparison that frequency estimations as minima of  $\Psi_1(f)$  or maxima of  $I(f)$  have errors with the upper bound  $\delta f = (2N\tilde{h})^{-1}$ . We have  $\delta f = 0.03$  in our case. This value looks too much great as the accuracy estimate of the frequencies  $f_k^{(i)}$ .

Certain of the found frequencies admit the obvious interpretation. The frequencies  $f_2^{(1)} \approx f_2^{(3)} \approx 0.37$  are caused by spacecraft orbital motion. The orbital frequency  $f_{\text{orb}}$  (the reciprocal quantity to the orbital period) equals 0.185 so

$$f_2^{(1)} \approx f_2^{(3)} \approx 2f_{\text{orb}}. \quad (9)$$

Return to formulas (3). The motion, which they describe, is called the nutational motion and its circular frequency  $p|\Omega|$  is called the nutation frequency. This circular frequency corresponds to the cyclic frequency  $f_{\text{nut}} = p|\Omega|/2\pi$  and we have  $f_{\text{nut}} = 2.341$  for interval 13. Hence,

$$f_8^{(1)} \approx f_{\text{nut}}, \quad f_{16}^{(2)} \approx f_{16}^{(3)} \approx 2f_{\text{nut}}. \quad (10)$$

Just the harmonic with the greatest amplitude has the frequency  $f_{\text{nut}}$ . The spacecraft nutational motion causes it. This result agrees with formula (1), where the first two terms predominate.

To interpret some other frequencies, let us assume that the spacecraft performs exact Euler's regular precession of an axisymmetric rigid body. Then we have to put  $I_2 = I_3$  in (3). Euler's precession is described usually by the nutation angle  $\mathcal{G}$ , the precession angle  $\phi_1$  and the angle  $\phi_2$  of a proper rotation, the quantities  $\mathcal{G}$ ,  $\dot{\phi}_1$ , and  $\dot{\phi}_2$  being constants in the exact precession. *Foton M-2* had [3]

$$\tan \mathcal{G} \approx \frac{W}{(1-p)\Omega}, \quad \dot{\phi}_1 \approx \frac{(1-p)\Omega}{\cos \mathcal{G}}, \quad \dot{\phi}_2 \approx p\Omega.$$

A vector that is a constant in the absolute space has time-dependent components in the system  $x_1x_2x_3$ . These components are sums of constant terms and four harmonics with the frequencies

$$f_{\text{pr}} = \frac{|\dot{\phi}_1|}{2\pi}, \quad f_{\text{nut}} = \frac{|\dot{\phi}_2|}{2\pi}, \quad f_{\text{rot}} = f_{\text{pr}} + f_{\text{nut}}, \quad f'_{\text{rot}} = |f_{\text{pr}} - f_{\text{nut}}|.$$

The amplitudes of the harmonics have the order  $O(\mathcal{G})$ ,  $O(\mathcal{G})$ ,  $O(1)$ , and  $O(\mathcal{G}^2)$  respectively when  $\mathcal{G} \rightarrow 0$ . There are  $\mathcal{G} \approx 21^\circ$ ,  $f_{\text{pr}} = 0.904$ ,  $f_{\text{rot}} = 3.247$ ,  $f'_{\text{rot}} = 1.438$  in our example. The harmonic with the frequency  $f_{\text{rot}}$  proved to be appreciable. We see in Table 2 that

Table 2. Frequencies and amplitudes of harmonic components in the calculated and measured accelerations. Interval 13

$k$	Frequency interpretation	$b'_1$		$b'_2$		$b'_3$		$b_1$		$b_2$		$b_3$	
		$f_k^{(1)}$	$A_k^{(1)}$	$f_k^{(2)}$	$A_k^{(2)}$	$f_k^{(3)}$	$A_k^{(3)}$	$f_k^{(1)}$	$A_k^{(1)}$	$f_k^{(2)}$	$A_k^{(2)}$	$f_k^{(3)}$	$A_k^{(3)}$
1								0.158	0.983				
2	$2f_{\text{orb}}$	0.371	2.011			0.367	0.531						
3		0.509	1.681										
4								0.698	0.699				
5		0.862	1.357										
6				2.044	0.478	2.035	0.600						
7										2.215	0.214	2.215	0.173
8	$f_{\text{nut}}$	2.376	20.05					2.375	20.22	2.374	0.674	2.375	0.785
9				2.535	0.440	2.530	0.655			2.536	0.206	2.536	0.158
10		2.683	1.255	2.725	0.588	2.720	0.926			2.705	0.204	2.705	0.168
11	$f_{\text{rot}} - 2f_{\text{orb}}$	2.867	2.280	2.887	2.621	2.887	4.475	2.924	2.387	2.891	0.819	2.892	0.664
12	$f_{\text{rot}} - f_{\text{orb}}$			3.074	1.884	3.075	1.860			3.075	2.070	3.075	1.694
13	$f_{\text{rot}}$			3.251	2.018	3.249	2.948	3.223	1.691	3.261	0.764	3.262	0.614
14										3.371	0.212	3.370	0.174
15								3.769	0.790				
16	$2f_{\text{nut}}$			4.746	0.632	4.750	0.606			4.751	0.523	4.751	0.643
17										5.300	0.210	5.300	0.259
18				6.143	0.474	6.147	0.357			6.145	0.364	6.145	0.447

$$f_{13}^{(2)} \approx f_{13}^{(3)} \approx f_{\text{rot}}. \quad (11)$$

We see also that

$$f_{12}^{(2)} \approx f_{12}^{(3)} \approx f_{\text{rot}} - f_{\text{orb}}, \quad f_{11}^{(1)} \approx f_{11}^{(2)} \approx f_{11}^{(3)} \approx f_{\text{rot}} - 2f_{\text{orb}}. \quad (12)$$

The harmonics with the frequencies  $f_{\text{rot}}$ ,  $f_{\text{rot}} - f_{\text{orb}}$ , and  $f_{\text{rot}} - 2f_{\text{orb}}$  can be explained by the last two terms in formula (1). In particular, the components of the last term that describes the atmosphere drag are presented in the geocentric absolute coordinate system by periodical functions with the orbital period. The second column in Table 2 summarizes our interpretation of some found frequencies.

We performed in the same way the spectral analysis of the functions  $b_i(t)$  plotted in Fig. 2a. Its results are presented in Tables 2 and Figs. 6, 7. We omitted plots relating to the function  $b_3(t)$  because it has the same frequency properties as  $b_2(t)$ . Accuracy characteristics of the found harmonics are following. The frequency  $f_8^{(1)}$  has the least standard deviation equal to 0.00011; standard deviations of the frequencies  $f_{11}^{(1)}$  and  $f_k^{(2,3)}$  ( $k = 8, 11, 12, 13, 16$ ) don't exceed 0.001; standard deviations of the other frequencies are within the limits  $0.001 \div 0.004$ . Standard deviations of the amplitudes  $A_k^{(1)}$  and  $A_k^{(2,3)}$  don't exceed 0.14 and 0.04 respectively.

One can see from Table 2 that the functions  $b_i(t)$  contain harmonics with about the same frequencies as the functions  $b'_i(t)$ . Therefore we used the same principle of the frequency numbering. The close frequencies are in the same line in Table 2. It is not surprising that the frequencies of functions  $b_i(t)$  satisfy the relations (9) – (12). However amplitudes of some corresponding harmonics in  $b_i(t)$  and  $b'_i(t)$  differ markedly. The greatest discrepancy of amplitudes takes place for harmonics with the frequencies  $f_{11}^{(2,3)}$  and  $f_{13}^{(2,3)}$ . There is only one good coincidence of amplitudes. It takes place for harmonics with the frequency  $f_8^{(1)} \approx f_{\text{nut}}$ . We see some coincidence in the case of frequencies  $f_{12}^{(2,3)}$ . Some discrepancy in the case of frequencies  $f_{16}^{(2,3)}$  and  $f_{18}^{(2,3)}$  can be explained by our pared-down using the TAS3 geometrical characteristics. The single-axis sensors for different directions had slightly different coordinates in this device whereas we use the same coordinates for each sensor.

It is worth to note that the discrepancy between corresponding frequencies of functions  $b_i(t)$  and  $b'_i(t)$  are distinctly smaller than errors in their interpretation in terms of  $f_{\text{rot}}$ ,  $f_{\text{nut}}$  and  $f_{\text{orb}}$ . Possibly, the inaccuracy of the interpretation is caused by some fine details of the motion.

Now, we turn to the spectral analysis of the components of the magnetic field strength. We investigated the functions  $h_i(t)$  calculated by formulas (2) and plotted in Fig. 1a. The investigation of the functions  $\hat{h}_i(t)$  gave the same results.

The analysis was made according to the scheme above. Its results are presented in Table 3 and Figs. 8, 9. The table and figures are arranged in the same manner as Table 2 and Figs. 4 – 7. The functions  $h_2(t)$  and  $h_3(t)$  have the same frequency properties, so we cited the plots for  $h_2(t)$  only. The quantities  $f_1^{(1)}$  and  $A_1^{(1)}$  in Table 3 have the standard deviations equal to 0.0062 and  $7000\gamma$  respectively. The frequencies  $f_3^{(1)}$  and  $f_{11}^{(2,3)}$  have the least standard deviations equal to 0.00019; standard deviations of the frequencies  $f_4^{(1)}$  and  $f_{12}^{(2,3)}$  don't exceed 0.0004; standard deviations of the other frequencies are within the limits  $0.0005 \div 0.003$ . Standard deviations of the amplitudes  $A_k^{(i)}$ , except  $A_1^{(1)}$ , don't exceed  $300\gamma$ .

The functions  $h_i(t)$  contain some harmonics with about the same frequencies as the functions  $b'_i(t)$  and  $b_i(t)$ . The first column of Table 3 gives in brackets the number of a close frequency from Table 2. Therefore it was not surprising that some frequencies, found in the functions  $h_i(t)$ , admit the obvious interpretation. Namely, we have the relations

$$f_{11}^{(2,3)} \approx f_{\text{rot}} - 2f_{\text{orb}}, \quad f_{12}^{(2,3)} \approx f_{\text{rot}} - f_{\text{orb}}, \quad f_3^{(1)} \approx 2f_{\text{orb}}, \quad f_4^{(1)} \approx 3f_{\text{orb}}$$

for frequencies of harmonics with large amplitudes and we have the relations

$$f_1^{(1)} \approx f_{\text{orb}}, \quad f_8^{(2,3)} \approx f_{\text{nut}}$$

for frequencies of harmonics with small amplitudes.

The frequencies  $f_{\text{rot}} - 2f_{\text{orb}}$  and  $f_{\text{rot}}$  appear both in the functions  $b'_{2,3}(t)$  and in the functions  $b_{2,3}(t)$ . But their presence in  $b'_{2,3}(t)$  is much more greater – the corresponding harmonics have much more greater amplitudes. It is worth to compare this fact with the following one. The frequency  $f_{\text{rot}} - f_{\text{orb}}$  is present in functions  $b'_{2,3}(t)$  and  $b_{2,3}(t)$  too; the amplitudes of corresponding harmonics are approximately equal in all these functions and are twice greater than amplitudes of harmonics with frequencies  $f_{\text{rot}} - 2f_{\text{orb}}$ ,  $f_{\text{rot}}$  in  $b_{2,3}(t)$ . Thus transition  $b_{2,3}(t) \rightarrow b'_{2,3}(t)$  doesn't change the amplitudes for the frequency  $f_{\text{rot}} - f_{\text{orb}}$ , which is absent in the functions  $h_i(t)$ , and essentially increases the amplitudes for the frequencies  $f_{\text{rot}} - 2f_{\text{orb}}$ ,  $f_{\text{rot}}$ , which are present in the functions  $h_{2,3}(t)$ . This situation is illustrated by comparison of Figs. 5a, 7a, and 9a. The comparison shows that the function  $b'_2(t)$  inherits the frequencies from the functions  $b_2(t)$  and  $h_2(t)$ . The same inheritance takes place in the case of functions  $b'_3(t)$ ,  $b_3(t)$  and  $h_3(t)$  (compare corresponding columns in Tables 2, 3). The analogous inheritance in the case of functions  $b'_1(t)$ ,  $b_1(t)$ , and  $h_1(t)$  is not so pronounced (see Figs. 4a, 6a, and 8a) against a background of the large amplitudes of the harmonics with the frequency  $f_{\text{nut}}$  in  $b'_1(t)$  and  $b_1(t)$ . But if we calculate amplitude ratios for harmonics with frequencies closed to  $2f_{\text{rot}}$  in  $b'_1(t)$  and  $h_1(t)$ , we find the influence of the

magnetic field has here the same order as in the case of the functions  $b'_{2,3}(t)$  and  $h_{2,3}(t)$ . Quantitative characteristics of the influence will be described below.

Table 3. Frequencies and amplitudes of harmonic components in the magnetic field strength.

$k$	Frequency interpretation	$h_1$		$h_2$		$h_3$	
		$f_k^{(1)}$	$A_k^{(1)}, \gamma$	$f_k^{(2)}$	$A_k^{(2)}, \gamma$	$f_k^{(3)}$	$A_k^{(3)}, \gamma$
1		0.026	13960				
2(1)	$f_{\text{orb}}$	0.193	3297				
3(2)	$2f_{\text{orb}}$	0.339	20240				
4(3)		0.510	13164				
5(4)		0.700	1775				
6(5)		0.868	6032				
7(6)				2.039	3697	2.039	3707
8(8)	$f_{\text{nut}}$			2.365	3362	2.364	3394
9(9)				2.526	3892	2.526	3851
10(10)				2.717	5831	2.717	5849
11(11)	$f_{\text{rot}} - 2f_{\text{orb}}$			2.887	28042	2.887	28067
12(13)	$f_{\text{rot}}$			3.245	14010	3.245	14011
13				3.433	1648	3.433	1671
14				3.566	2790	3.566	2770

The analogous analysis was made for interval 9 from Table 1 to investigate the influence of variations of  $\Omega$  on the results obtained. New results proved to be in a good agreement with the previous ones. We have  $f_{\text{rot}} = 2.586$  and  $f_{\text{nut}} = 1.898$  based on  $\Omega$  for interval 9. The transition  $b_{2,3}(t) \rightarrow b'_{2,3}(t)$  increases the amplitudes for frequencies  $f_{\text{rot}} - 2f_{\text{orb}} \approx 2.34$  and  $f_{\text{rot}} \approx 2.70$  which are present in the functions  $h_{2,3}(t)$ . The transition  $b_1(t) \rightarrow b'_1(t)$  increases the amplitude for frequency  $2f_{\text{orb}}$ , which is present in the function  $h_1(t)$ .

**5. Correction of filtered TAS3 measurement data.** As long as the main frequencies of the functions  $b'_i(t)$  are obtained by joining up the main frequencies of the functions  $b_i(t)$  and  $h_i(t)$ , we can assume that the Earth magnetic field influenced upon TAS3 measurements linearly. This assumption gives hope to us that TAS3 filtered data can be corrected by the formulas

$$b'_i - \sum_{j=1}^3 m_{ij} h_j \rightarrow b'_i \quad (i = 1, 2, 3),$$

where  $m_{ij}$  are constants. We suppose here and below in this Section that the sign of the component  $b'_2$  has been changed.

If we make a correction for the magnetic field, it is naturally to make simultaneously some other corrections, namely, the correction for infra low-frequency errors, the correction for the shift of TAS3 time scale, the correction for the error in the spacecraft ballistic coefficient and the correction for misalignment of sensitive TAS3 axes with respect to the axes  $y_i$ . We specify the last correction by the vector  $\boldsymbol{\theta} = (\theta_1, \theta_2, \theta_3)$  of infinitesimal rotation of TAS3 sensitive axes with respect to the system  $y_1 y_2 y_3$ . The components of  $\boldsymbol{\theta}$  can be regarded both to the system  $y_1 y_2 y_3$  and to the system formed by sensitive axes of TAS3. The correction of the ballistic coefficient is specified by means of multiplication of it by the factor  $\chi$ :  $\chi c \rightarrow c$ . This correction compensates short time variations of  $c$  and  $\rho_a$  within a long interval in which  $c$  was defined. Taking into account all these corrections and assuming they allow removing all possible errors, we can write

$$\begin{aligned}
b'_1(t) + \theta_2 b'_3(t) - \theta_3 b'_2(t) - Z_1(t) - \sum_{j=1}^3 m_{1j} h_j(t + \tau) &= \\
= \sum_{j=1}^3 c_{1j}(t + \tau) [x_j^{(1)} + x_j] + \chi b_1^{(a)}(t + \tau), \\
b'_2(t) + \theta_3 b'_1(t) - \theta_1 b'_3(t) - Z_2(t) - \sum_{j=1}^3 m_{2j} h_j(t + \tau) &= \quad (13) \\
= \sum_{j=1}^3 c_{2j}(t + \tau) [x_j^{(2)} + x_j] + \chi b_2^{(a)}(t + \tau), \\
b'_3(t) + \theta_1 b'_2(t) - \theta_2 b'_1(t) - Z_3(t) - \sum_{j=1}^3 m_{3j} h_j(t + \tau) &= \\
= \sum_{j=1}^3 c_{3j}(t + \tau) [x_j^{(3)} + x_j] + \chi b_3^{(a)}(t + \tau),
\end{aligned}$$

$$Z_i(t) = A_{K+1}^{(i)} + (t - t_0) A_{K+2}^{(i)} + \sum_{k=1}^K A_k^{(i)} \sin \frac{\pi k(t - t_0)}{N \tilde{h}} \quad (i = 1, 2, 3).$$

Here, the functions  $Z_i(t)$  compensate infra low-frequency errors in filtered data,  $\tau$  is the shift of TAS3 time scale with respect to the time scale used for description of spacecraft attitude motion, the functions  $c_{ij}(t)$  and  $b_j^{(a)}(t)$  are defined by relations (see (1),  $\mathbf{e}_i$  are unit vectors along the axes  $y_i$ )

$$\mathbf{e}_i \times \dot{\boldsymbol{\omega}} + \boldsymbol{\omega} \times (\mathbf{e}_i \times \boldsymbol{\omega}) + \frac{\mu_e}{|\mathbf{R}|^3} \left[ \frac{3(\mathbf{R} \cdot \mathbf{e}_i) \mathbf{R}}{|\mathbf{R}|^2} - \mathbf{e}_i \right] = \sum_{j=1}^3 c_{ji} \mathbf{e}_j, \quad c \rho_a |\mathbf{v}| \mathbf{v} = \sum_{j=1}^3 b_j^{(a)} \mathbf{e}_j,$$

the quantities  $x_j$  set the origin of TAS3 coordinate system with respect to the spacecraft mass center,  $x_j^{(k)}$  ( $j = 1, 2, 3$ ) are the coordinates of the TAS3 sensor for

the axis  $y_k$  in the TAS3 own coordinate system,

$$\begin{aligned} x_1^{(1)} &= -56.2 \text{ mm}, & x_2^{(1)} &= 48.5 \text{ mm}, & x_3^{(1)} &= -57.0 \text{ mm}, \\ x_1^{(2)} &= -36.5 \text{ mm}, & x_2^{(2)} &= 22.3 \text{ mm}, & x_3^{(2)} &= -70.5 \text{ mm}, \\ x_1^{(3)} &= -31.0 \text{ mm}, & x_2^{(3)} &= 48.5 \text{ mm}, & x_3^{(3)} &= -27.8 \text{ mm}, \end{aligned}$$

We considered relations (13) as equations for determining the unknown quantities  $\theta_i$ ,  $x_i$ ,  $A_k^{(i)}$ ,  $m_{ij}$ ,  $\chi$ , and  $\tau$ . We look for these quantities in the following way. Let  $\tau$  be given. We consider relations (13) at the points  $\tilde{t}_n$  defined by formulas (5). The quantities  $b'_i(\tilde{t}_n)$  are calculated at filtration and we don't exclude the infra low-frequency component from them because this corrections are provided by functions  $Z_i(t)$ . The quantities  $c_{ij}(\tilde{t}_n + \tau)$  and  $b_i^{(a)}(\tilde{t}_n + \tau)$  are calculated by interpolation using finite Fourier series. Those series were constructed beforehand basing on the proper solution of spacecraft motion equations. We obtained as a result the overdetermined linear system with the unknown quantities  $\theta_i$ ,  $x_i$ ,  $A_k^{(i)}$ ,  $m_{ij}$ , and  $\chi$ . We treat the problem of finding its solution as a standard linear regression problem. We solve it by the least squares method for each  $\tau$  at points of the uniform grid with the step 1 s and calculate the standard deviation  $\sigma_b = \sigma_b(\tau)$  of discrepancies in (13). The value  $\tau_* = \arg \min \sigma_b(\tau)$  is considered to be the required estimate of  $\tau$ . The solution of the regression problem at  $\tau = \tau_*$  gives us the required estimates of the quantities listed above. The standard deviations of those quantities, calculated at  $\tau = \tau_*$  in the framework of a linear regression problem previously mentioned, are adopted as accuracy characteristics of the found estimates. We emphasize the standard deviations are calculated at fixed  $\tau$ , which is supposed to be known, and are so-called conditional standard deviations. The unconditional standard deviation  $\sigma_\tau$  of the estimate  $\tau_*$  is calculated by the formula

$$\sigma_\tau^2 = 2\sigma_b^2(\tau_*) \left[ (3N - 3K - 23) \frac{d^2 \sigma_b^2(\tau_*)}{d\tau^2} \right]^{-1}.$$

The results of solution of the regression problem are presented in Table 4 and Figs. 10 – 12. These results were obtained for some intervals from Table 1. They were obtained at  $K = 10$  but they almost coincide with the results for  $K = 5$  and  $K = 3$ . Table 4 contains the estimates of the quantities  $\tau$ ,  $x_i$ ,  $\chi$ ,  $\theta_i$ , and  $m_{ij}$  as well as their standard deviations. The unit of  $\theta_i$  and  $\sigma_{\theta_i}$  is radian, the unit of  $m_{ij}$  and  $\sigma_{m_{ij}}$  is  $10^{-7} \text{ m}/(\text{s}^2 \cdot \text{Oe})$ .

Figs. 10a, 11a, and 12a contain the plots of the functions  $\hat{b}_i(t)$  and  $b_i(t)$  ( $i = 1, 2, 3$ ) defined by the left-hand sides and right-hand sides of formulas (13). Thick lines depict the plots of the functions  $b_i(t)$ ; fine lines depict the plots of the

Table 4. Estimations of TAS3 adjusting parameters. The unit of  $m_{ij}$  and  $\sigma_{mij}$  is  $10^{-7} \text{ m}/(\text{s}^2 \cdot \text{Oe})$ 

Interval	$\sigma_b,$ $10^{-6} \text{ m/s}^2$	$\tau,$ s	$\sigma_\tau,$ s	$x_1,$ mm	$\sigma_{x1},$ mm	$x_2,$ mm	$\sigma_{x2},$ mm	$x_3,$ mm	$\sigma_{x3},$ mm	$\chi$	$\sigma_\chi$
1	0.764	-48	3.0	22.3	19	-121.0	5.5	-219.8	4.5	0.929	0.023
2	0.675	-37	2.4	-13.7	13	-96.9	2.9	-229.1	2.8	1.089	0.016
4	0.801	-22	2.5	-16.7	13	-109.8	2.5	-231.0	2.4	1.179	0.020
6	0.748	-32	1.7	1.6	12	-86.0	1.9	-227.2	1.9	1.043	0.020
8	0.781	-25	1.7	-7.0	5.0	-94.3	0.74	-241.2	0.73	1.095	0.015
9	0.999	-32	1.8	-8.1	5.8	-63.6	0.83	-238.8	0.82	0.939	0.016
10	0.742	-23	1.2	-8.4	4.1	-96.1	0.57	-235.8	0.57	0.900	0.012
11	0.745	-19	1.4	-10.9	4.3	-96.8	0.60	-226.1	0.60	1.078	0.013
12	0.952	-23	1.9	-9.8	6.0	-69.4	0.85	-236.4	0.84	0.895	0.017
13	0.734	-15	1.2	-7.8	4.6	-104.2	0.66	-229.8	0.64	1.040	0.014

Interval	$\theta_1$	$\sigma_{\theta 1}$	$\theta_2$	$\sigma_{\theta 2}$	$\theta_3$	$\sigma_{\theta 3}$	$m_{11}$	$\sigma_{m11}$	$m_{12}$	$\sigma_{m12}$	$m_{13}$	$\sigma_{m13}$
1	0.002	0.020	-0.039	0.017	0.0007	0.013	-189.2	2.9	-5.1	2.1	-87.2	3.5
2	0.040	0.013	0.014	0.011	0.020	0.0085	-197.9	1.9	-16.6	1.9	-101.8	2.3
4	-0.099	0.016	-0.010	0.0099	0.006	0.0076	-184.6	1.7	-15.8	1.9	-97.2	2.4
6	0.060	0.015	-0.017	0.0089	0.040	0.0064	-191.0	1.6	-5.3	1.7	-99.5	2.2
8	-0.008	0.012	-0.034	0.0037	0.026	0.0025	-186.9	2.8	-16.7	1.4	-98.2	1.5
9	0.132	0.014	-0.010	0.0043	0.018	0.0028	-188.7	2.9	-1.8	1.9	-105.2	2.0
10	-0.026	0.011	-0.033	0.0030	0.024	0.0019	-189.0	2.5	-14.9	1.4	-100.8	1.5
11	0.022	0.011	-0.026	0.0032	0.012	0.0021	-178.8	3.0	-13.5	1.4	-96.4	1.5
12	0.161	0.015	-0.021	0.0044	0.022	0.0029	-185.9	3.1	-6.6	1.9	-101.8	2.0
13	-0.043	0.013	-0.040	0.0034	0.013	0.0022	-184.1	2.6	-18.1	1.4	-99.6	1.5

Table 4 (continuation). Estimations of TAS3 adjusting parameters. The unit of  $m_{ij}$  and  $\sigma_{mij}$  is  $10^{-7} \text{ m}/(\text{s}^2 \cdot \text{Oe})$ 

Interval	$m_{21}$	$\sigma_{m21}$	$m_{22}$	$\sigma_{m22}$	$m_{23}$	$\sigma_{m23}$	$m_{31}$	$\sigma_{m31}$	$m_{32}$	$\sigma_{m32}$	$m_{33}$	$\sigma_{m33}$
1	6.6	3.2	-104.4	1.6	-26.7	3.9	-21.9	3.6	-1.9	2.3	-169.4	2.8
2	3.1	2.4	-105.9	1.7	-29.2	2.5	-14.5	2.6	-14.5	2.0	-170.9	1.8
4	11.6	2.1	-111.4	1.7	-35.2	3.2	-15.2	2.4	-10.9	2.4	-172.0	1.8
6	7.8	1.9	-108.0	1.6	-26.5	3.0	-18.3	2.2	-17.2	2.2	-176.0	1.9
8	2.8	2.8	-111.7	1.5	-23.9	2.3	-11.6	2.8	-21.7	1.8	-171.8	1.4
9	2.2	2.9	-98.4	1.9	-6.8	2.9	-10.7	3.0	-9.8	2.3	-184.8	1.9
10	10.3	2.5	-106.3	1.5	-26.0	2.2	-25.4	2.6	-11.3	1.8	-174.7	1.4
11	10.6	3.0	-106.9	1.5	-22.6	2.2	-20.3	3.0	-28.8	1.8	-180.5	1.4
12	6.7	3.1	-96.4	1.9	-4.2	3.1	-15.3	3.2	-18.6	2.4	-188.1	1.8
13	2.3	2.6	-115.4	1.5	-28.2	2.5	-19.7	2.6	-20.1	1.9	-170.2	1.4

Table 5. Estimations of TAS3 adjusting parameters. The unit of  $m_{ij}$  and  $\sigma_{mij}$  is  $10^{-7} \text{ m}/(\text{s}^2 \cdot \text{Oe})$ 

Interval	$\sigma_b,$ $10^{-6} \text{ m/s}^2$	$\tau,$ s	$\sigma_\tau,$ s	$x_1,$ mm	$\sigma_{x1},$ mm	$x_2,$ mm	$\sigma_{x2},$ mm	$x_3,$ mm	$\sigma_{x3},$ mm	$\chi$	$\sigma_\chi$
8	0.820	-28	0.82	25.4	3.5	-83.3	0.76	-242.1	0.77	1.105	0.016
9	1.024	-26	0.79	16.2	3.9	-84.7	0.84	-236.8	0.84	0.937	0.016
10	0.793	-26	0.65	21.7	2.8	-83.5	0.61	-237.0	0.61	0.901	0.013
11	0.766	-19	0.57	16.3	2.9	-96.0	0.61	-226.1	0.62	1.083	0.013
12	0.988	-18	0.74	26.0	4.1	-89.9	0.87	-233.9	0.87	0.882	0.017
13	0.763	-19	0.64	25.0	3.1	-85.8	0.66	-232.4	0.67	1.035	0.015

Interval	$m_{11}$	$\sigma_{m11}$	$m_{12}$	$\sigma_{m12}$	$m_{13}$	$\sigma_{m13}$
8	-190.6	3.0	-16.0	1.5	-104.4	1.5
9	-188.2	3.0	-13.0	1.9	-106.2	1.9
10	-190.5	2.7	-13.1	1.5	-106.4	1.5
11	-177.3	3.1	-15.8	1.4	-100.5	1.4
12	-184.5	3.2	-18.1	1.9	-104.2	1.9
13	-182.4	2.7	-13.7	1.5	-107.2	1.5

Interval	$m_{21}$	$\sigma_{m21}$	$m_{22}$	$\sigma_{m22}$	$m_{23}$	$\sigma_{m23}$	$m_{31}$	$\sigma_{m31}$	$m_{32}$	$\sigma_{m32}$	$m_{33}$	$\sigma_{m33}$
8	6.8	2.9	-108.4	1.5	-28.0	1.4	-5.5	2.9	-16.1	1.4	-171.2	1.5
9	4.4	2.9	-99.9	1.9	-20.0	1.9	-9.2	2.9	-11.5	1.9	-180.7	1.9
10	15.1	2.7	-104.8	1.5	-27.5	1.5	-19.6	2.7	-6.7	1.5	-173.7	1.5
11	11.9	3.0	-106.9	1.4	-26.2	1.4	-16.3	3.0	-26.6	1.4	-179.0	1.4
12	8.3	3.2	-99.8	1.9	-22.4	1.9	-12.7	3.2	-17.6	1.9	-182.6	1.9
13	4.6	2.6	-111.6	1.4	-29.0	1.5	-12.9	2.6	-12.6	1.5	-169.8	1.5

Table 6. Estimations of TAS3 adjusting parameters. The unit of quantities  $m_{ij}$  and  $\sigma_{mij}$  is  $10^{-7} \text{ m}/(\text{s}^2 \cdot \text{Oe})$ 

Interval	$\sigma_b,$ $10^{-6} \text{ m/s}^2$	$\tau,$ s	$\sigma_\tau,$ c	$x_1,$ mm	$\sigma_{x1},$ mm	$x_2,$ mm	$\sigma_{x2},$ mm	$x_3,$ mm	$\sigma_{x3},$ mm	$\chi$	$\sigma_\chi$
8	0.781	-25	0.79	-7.0	5.0	-94.3	0.74	-241.2	0.73	1.095	0.015
9	1.005	-25	0.79	-6.8	5.8	-88.8	0.84	-236.4	0.83	0.930	0.016
10	0.742	-24	0.61	-8.9	4.1	-92.2	0.58	-236.3	0.57	0.900	0.012
11	0.745	-18	0.56	-10.3	4.3	-100.7	0.60	-225.4	0.60	1.077	0.013
12	0.958	-16	0.72	-6.9	6.0	-99.3	0.86	-232.7	0.85	0.874	0.017
13	0.734	-17	0.62	-8.9	4.6	-95.5	0.65	-231.3	0.64	1.036	0.014

Interval	$\theta_2$	$\sigma_{\theta 2}$	$\theta_3$	$\sigma_{\theta 3}$	$m_{11}$	$\sigma_{m11}$	$m_{12}$	$\sigma_{m12}$	$m_{13}$	$\sigma_{m13}$
8	-0.035	0.0037	0.026	0.0024	-186.9	2.8	-16.7	1.4	-98.2	1.5
9	-0.023	0.0043	0.018	0.0028	-188.2	2.9	-11.9	1.9	-102.4	2.0
10	-0.032	0.0030	0.024	0.0019	-189.0	2.5	-13.3	1.4	-101.2	1.5
11	-0.027	0.0032	0.011	0.0021	-178.7	3.0	-14.9	1.4	-95.9	1.5
12	-0.034	0.0044	0.022	0.0029	-185.5	3.1	-17.6	1.9	-98.3	2.0
13	-0.037	0.0034	0.013	0.0022	-184.2	2.6	-14.6	1.4	-100.7	1.5

Interval	$m_{21}$	$\sigma_{m21}$	$m_{22}$	$\sigma_{m22}$	$m_{23}$	$\sigma_{m23}$	$m_{31}$	$\sigma_{m31}$	$m_{32}$	$\sigma_{m32}$	$m_{33}$	$\sigma_{m33}$
8	2.8	2.8	-111.4	1.4	-22.7	1.4	-11.5	2.8	-22.5	1.4	-171.9	1.4
9	1.3	2.9	-101.6	1.9	-19.0	1.9	-13.3	3.0	-14.4	1.9	-181.6	1.9
10	10.8	2.5	-105.4	1.4	-23.5	1.4	-24.8	2.6	-11.2	1.4	-175.1	1.4
11	10.2	3.0	-107.9	1.4	-24.5	1.4	-20.8	3.0	-29.4	1.4	-179.9	1.4
12	4.6	3.1	-100.9	1.9	-18.8	1.9	-18.6	3.2	-23.6	1.9	-183.4	1.9
13	2.8	2.6	-113.4	1.4	-25.1	1.4	-19.0	2.6	-18.5	1.4	-171.3	1.4

functions  $\hat{b}_i(t)$ . Figs. 10b, 11b, and 12b contain the plots of the differences  $\Delta b_i(t) = \hat{b}_i(t) - b_i(t)$  ( $i=1, 2, 3$ ). The functions, obtained in both ways, are in a good agreement with each other. The differences  $\Delta b_i(t)$  are small and look as irregular oscillations with sufficiently high frequencies. The figures illustrate only intervals 2, 6 and 13 but they give an idea about all intervals in Table 1.

The values of  $\sigma_b$  in Table 4 are close for all intervals but the estimates of the most interesting fitted parameters  $x_i$  were stabilized only since interval 8 (see standard deviations  $\sigma_{x_i}$  in Table 4). The useful signal in measurement data was apparently lost against background of infra low-frequency errors in preceding intervals. One can see from Table 1 and Figs. 10a, 11a, and 12a that amplitudes of  $b_1$ , maximal values of  $|b_2|$ ,  $|b_3|$ , and frequencies of these functions increased coupled with  $\Omega$ . So, the low-frequency filtration enabled to extract the useful signal in  $b'_i$  starting the certain value of  $\Omega$ .

The weighted mean values of the parameters  $x_i$  in the last six rows of Table 4 are  $\bar{x}_1 = -8.7$  mm,  $\bar{x}_2 = -90.9$  mm,  $\bar{x}_3 = -233.8$  mm, the weights being proportional to  $\sigma_{x_i}^{-2}$ . The standard deviations of these mean values are  $\sigma_{\bar{x}_1} = 0.58$  mm,  $\sigma_{\bar{x}_2} = 7.0$  mm,  $\sigma_{\bar{x}_3} = 2.4$  mm. The mean values of the quantities  $\sigma_{x_i}$  in the last six rows of Table 4 are  $\bar{\sigma}_{x1} = 5.0$  mm,  $\bar{\sigma}_{x2} = 0.71$  mm,  $\bar{\sigma}_{x3} = 0.70$  mm. The analogous estimates for the factor  $\chi$  are  $\bar{\chi} = 0.993$ ,  $\sigma_{\bar{\chi}} = 0.065$ ,  $\bar{\sigma}_{\chi} = 0.014$ . The estimates turned out to be fairly accurate. So, the aerodynamic term in formula (1) was calculated correctly.

It is interesting to estimate misalignment of sensitive TAS3 axes with respect to the axes  $y_i$ . This misalignment is described by the angles  $\theta_i$ . The weighted mean values of these angles in the last six rows of Table 4 are  $\bar{\theta}_1 = 0.027(1.5^\circ)$ ,  $\bar{\theta}_2 = -0.029(1.7^\circ)$ ,  $\bar{\theta}_3 = 0.019(1.1^\circ)$ . The standard deviations of these mean values are  $\sigma_{\bar{\theta}_1} = 0.036$ ,  $\sigma_{\bar{\theta}_2} = 0.0045$ ,  $\sigma_{\bar{\theta}_3} = 0.0024$ . The mean values of the quantities  $\sigma_{\theta_i}$  in the last six rows of Table 4 are  $\bar{\sigma}_{\theta1} = 0.013$ ,  $\bar{\sigma}_{\theta2} = 0.0037$ ,  $\bar{\sigma}_{\theta3} = 0.0024$ . The estimates of the quantities  $\theta_2$  and  $\theta_3$  look fairly good. The estimate of  $\theta_1$  is not so exact.

Since the angles  $\theta_i$  were small, it is worth to solve our regression problem under the condition  $\theta_i = 0$  ( $i=1, 2, 3$ ). The results of solving this problem for the last six intervals of Table 1 are presented in Table 5. All these results were obtained under  $K=10$ . Table 5 is arranged analogously to Table 4. The values of  $\sigma_b$  in it are just a little larger than in Table 4 but estimates of the coordinate  $x_1$  differ visibly in these tables. In particular, we have for data in Table 5  $\bar{x}_1 = 21.5$  mm,  $\bar{x}_2 = -87.5$  mm,  $\bar{x}_3 = -234.1$  mm,  $\sigma_{\bar{x}_1} = 1.9$  mm,  $\sigma_{\bar{x}_2} = 2.0$  mm,  $\sigma_{\bar{x}_3} = 2.3$  mm,  $\bar{\sigma}_{x1} = 3.4$  mm,  $\bar{\sigma}_{x2} = 0.73$  mm,  $\bar{\sigma}_{x3} = 0.73$  mm. Of course, the difference in values of  $x_1$  is small in comparison with TAS3 dimensions but it is large in comparison with the values of  $\sigma_{x1}$ ,  $\sigma_{\bar{x}_1}$ , and  $\bar{\sigma}_{x1}$ . We point out also the decrease of the standard devia-

tions  $\sigma_\tau$  in Table 5 as against Table 4. Table 6 contains results of solving the regression problem under the conditions  $\theta_1 = 0$  and  $K = 10$  for the same intervals as in Table 5. The results occurred distinctly closer to data in Table 4 but the standard deviations  $\sigma_\tau$  remained small.

Now, we consider the estimates of coefficients  $m_{ij}$  and their standard deviations. The weighted mean values of these coefficients in the last six rows of Table 4 are

$$\|\bar{m}_{ij}\| = \begin{vmatrix} -185.8 & -13.3 & -99.8 \\ 5.8 & -107.1 & -20.6 \\ -17.6 & 19.0 & -177.0 \end{vmatrix}$$

$$\|\sigma_{\bar{m}_{ij}}\| = \begin{vmatrix} 1.5 & 2.8 & 2.3 \\ 1.6 & 3.1 & 4.3 \\ 2.3 & 2.9 & 3.0 \end{vmatrix}, \quad \|\bar{\sigma}_{m_{ij}}\| = \begin{vmatrix} 2.8 & 1.6 & 1.7 \\ 2.8 & 1.6 & 2.5 \\ 2.9 & 2.0 & 1.6 \end{vmatrix}.$$

The unit of these quantities are  $10^{-7} \text{ m}/(\text{s}^2 \cdot \text{Oe})$ . The analogous average characteristics for Tables 5 and 6 are close to these. One can see in Tables 4 – 6 that the differences between estimates of  $m_{ij}$  in different tables have the same order as appropriate  $\sigma_{m_{ij}}$ . The values of  $m_{ij}$  in Tables 4 – 6 show that the influence of the magnetic field is approximately the same for all components  $b'_i$

**6. Conclusion.** The investigation of TAS3 measurement data showed that this accelerometer was sufficiently exact and sensitive to measure quasi-steady accelerations. TAS3 was designed first of all for measuring high-frequency accelerations with sufficiently large amplitudes onboard spacecraft. Therefore extraction of a quasi-steady acceleration component from its measurement data demanded special efforts. In particular, we had to eliminate infra low-frequency errors and to make a correction for the influence of the Earth magnetic field. The infra low-frequency errors were apparently caused by a zero drift, a thermal influence, etc. TAS3 didn't have respective compensative facilities. Fortunately, the quasi-steady acceleration at the TAS3 location was sufficiently large and had appropriate frequencies as early as a few days after the beginning of the flight. Moreover, the time dependence of the quasi-steady acceleration could be described in the very convenient mathematical form owing to the specific attitude motion of the spacecraft. The influence of the Earth magnetic field upon TAS3 readings was very small and could not be taken into account in regular situations of the device operation. But quasi-steady accelerations have usually so small amplitudes that the correction needs. All listed facts caused the methods of processing the TAS3 measurement data in low-frequency range and enabled to show utmost opportunities of this accelerometer.

Our investigation demonstrated once again that the calculated way of determining the quasi-steady acceleration component is efficient. It gives detailed information about real though rather idealized accelerations in low-frequency range. This information can be very useful in analysis of acceleration measurement data.

Besides in some situations, this information alone gives an exact and complete description of low-frequency microgravity environment onboard spacecraft.

### References

1. Sazonov, V.V., Komarov, M.M., Polezhaev, V.I., Nikitin, S.A., Ermakov, M.K., Stazhkov, V.M., Zykov, S.G., Ryabukha, S.B., Acevedo, J., Liberman, E.: Microaccelerations on board the Mir orbital station and prompt analysis of gravitational sensitivity of convective processes of heat and mass transfer. *Cosmic research*, 1999, vol. 37, No. 1, pp. 80-94.
2. Abrashkin, V.I., Balakin, V.L., Belokonov, I.V., Voronov, K.E., Zaitsev, A.S., Ivanov, V.V., Kazakova, A.E., Sazonov, V.V., Semkin, N.D.: Uncontrolled attitude motion of the Foton-12 satellite and quasi-steady microaccelerations onboard it. *Cosmic research*, 2003, vol. 41, No. 1, pp. 31-50.
3. Abrashkin, V.I., Bogoyavlensky, N.L., Voronov, K.E., Kazakova, A.E., Puzin, Yu.Ya., Sazonov, V.V., Semkin, N.D., Chebukov, S.Yu.: Uncontrolled motion of the *Foton M-2* satellite and quasistatic microaccelerations on its board. *Cosmic research*, 2007, vol. 45, No. 5, pp. 424-444.
4. Abrashkin, V.I., Volkov, M.V., Egorov, A.V., Zaitsev, A.S., Kazakova, A.E., Sazonov, V.V.: An analysis of the low-frequency component in measurements of angular velocity and microacceleration onboard the Foton-12 satellite. *Cosmic research*, 2003, vol. 41, No. 6, pp. 593-611.
5. Abrashkin, V.I., Kazakova, A.E., Puzin, Yu.Ya., Sazonov, V.V., Chebukov, S.Yu. Determination of the spacecraft Foton M-2 attitude motion on measurements of the angular rates. Preprint, Keldysh Institute of Applied Mathematics, Russia Academy of Sciences, 2005, No. 110.
6. Hannan, E.J.: *Time series analysis*. Methuen & Co Ltd., London, John Wiley & Sons, New York (1960).
7. Terebizh, V. Yu.: *Time series analysis in astrophysics*. Nauka, Moscow

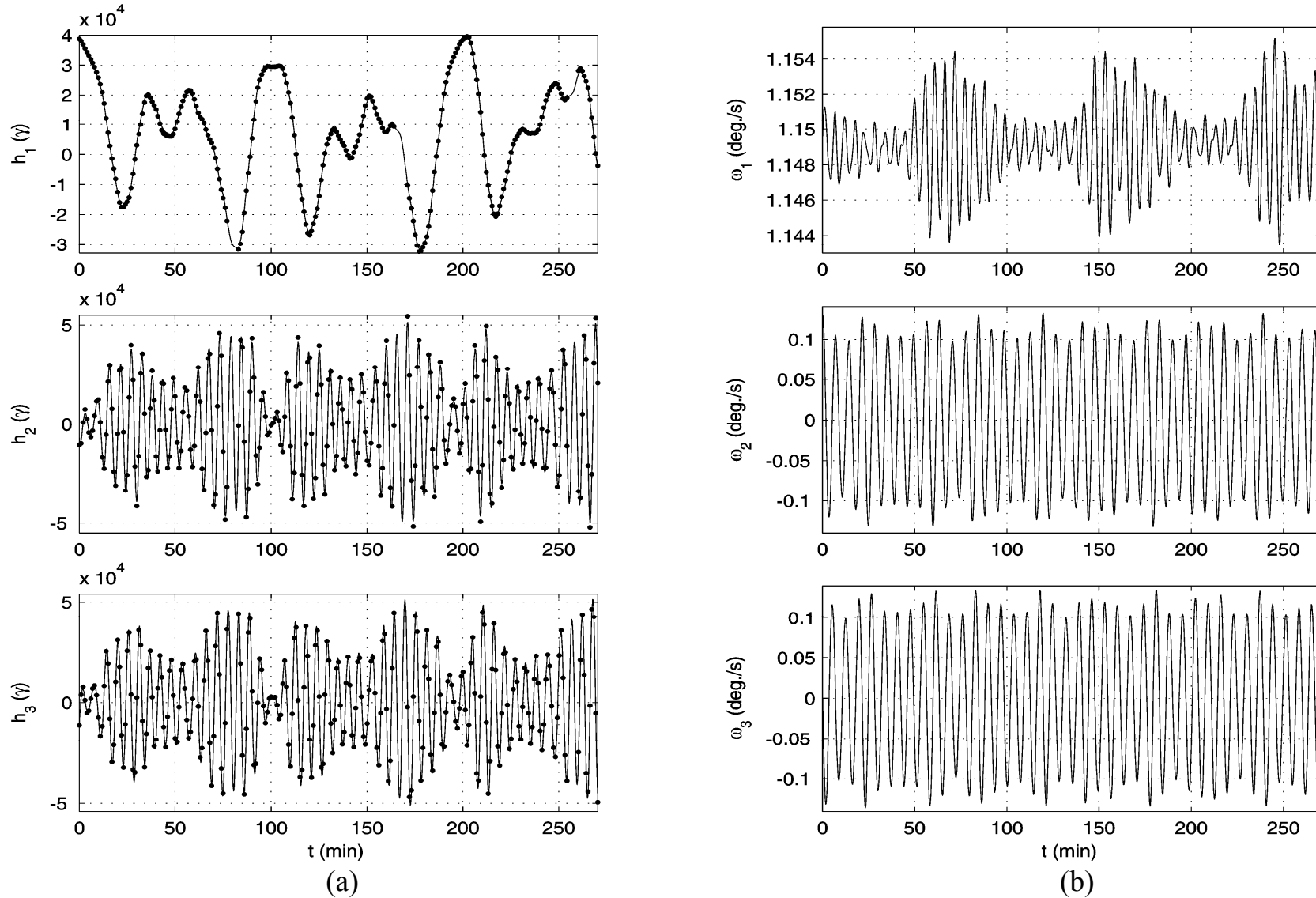


Fig. 1. On the reconstruction of the spacecraft attitude motion in interval 13: (a) the approximation of the magnetic field measurements, (b) the spacecraft angular rate. The instant  $t = 0$  in the plots corresponds to 09:21:20 UTC 09.06.2005,  $\sigma = 1147 \gamma$ ,  $\Omega = 1.1491 \text{ deg./s}$ ,  $\delta\Omega = 0.0021 \text{ deg./s}$ ,  $W = 0.1124 \text{ deg./s}$ ,  $\delta W = 0.0103 \text{ deg./s}$ .

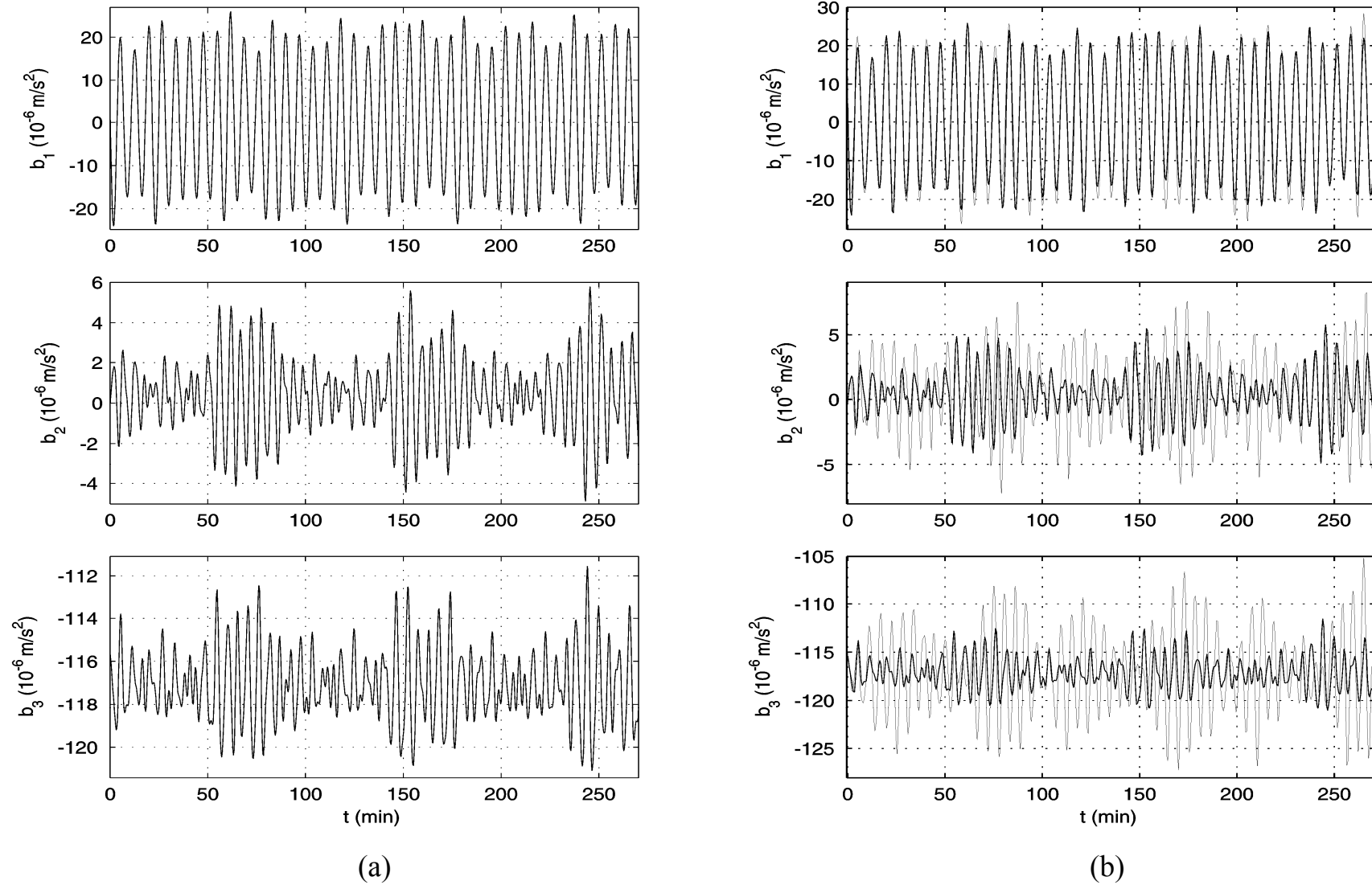


Fig. 2. The accelerations at the point of TAS3 location: (a) calculated for the motion in interval 13 (Fig. 1), (b) measured by TAS3 (bold-faced lines shifted to the left on 30s) and calculated for the motion in interval 13.

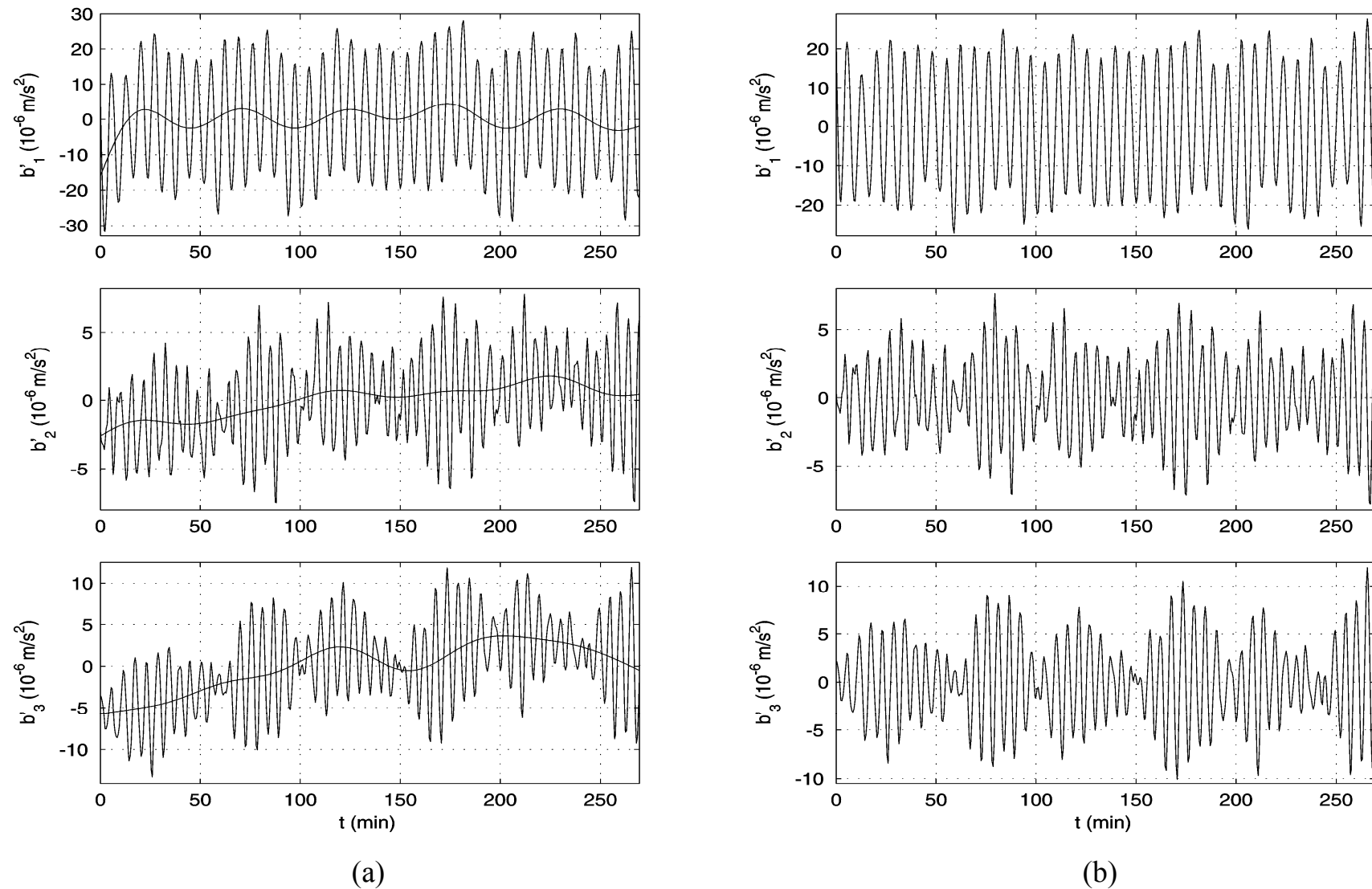
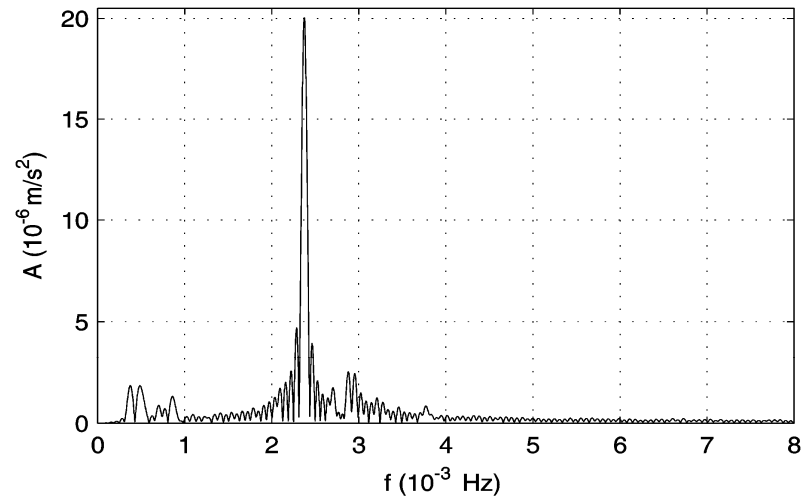
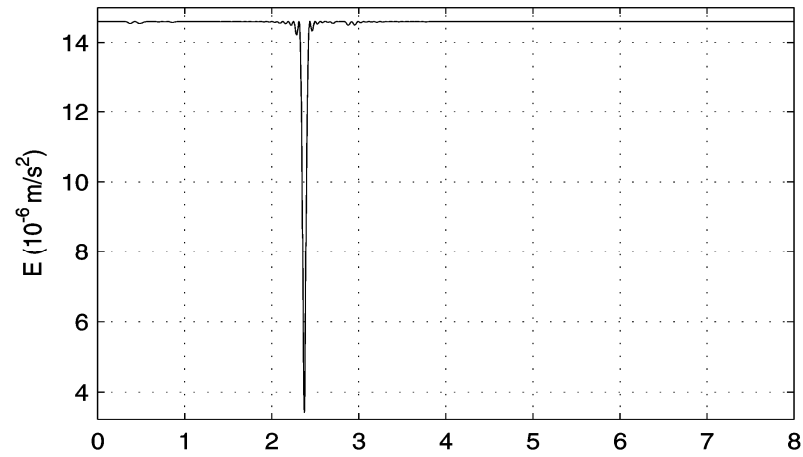
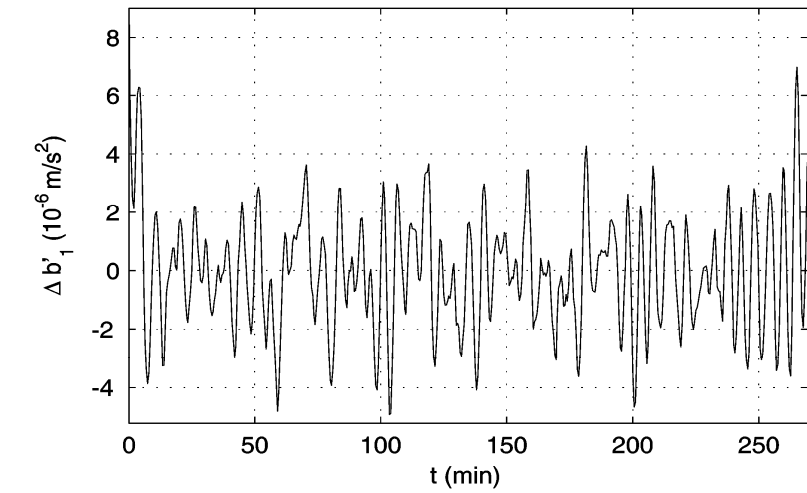
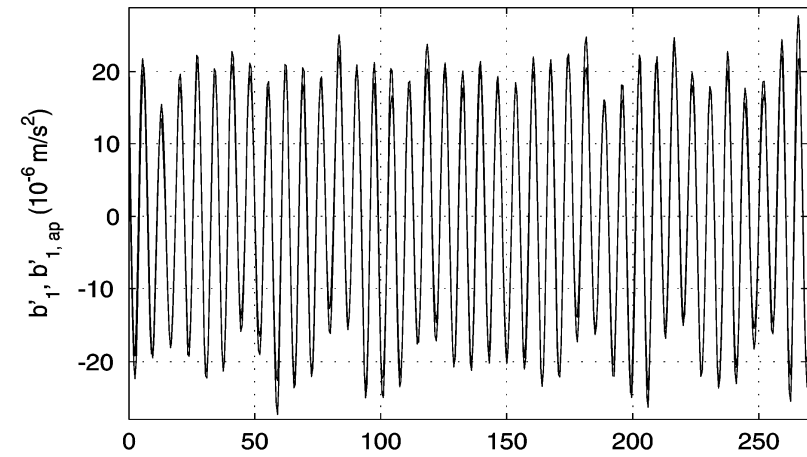


Fig. 3. Elimination of the ultra low-frequency component from the filtered TAS3 measurements in interval 13: (a) before elimination (fluent curves represent the ultra low-frequency component), (b) after elimination.

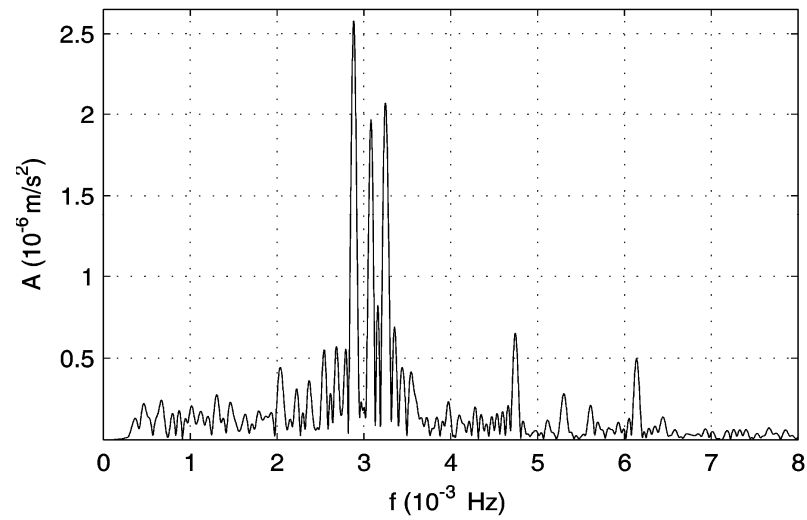
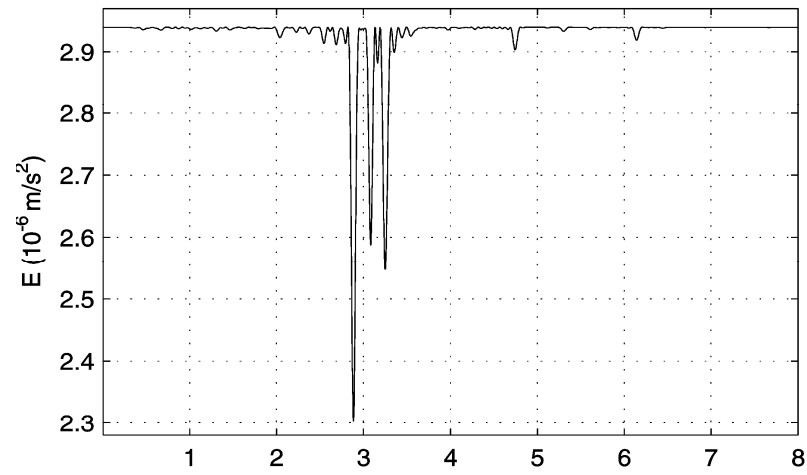


(a)

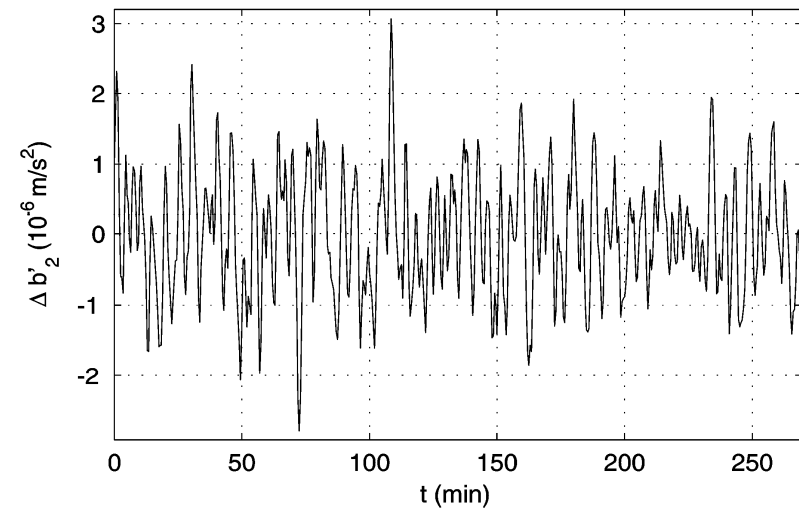
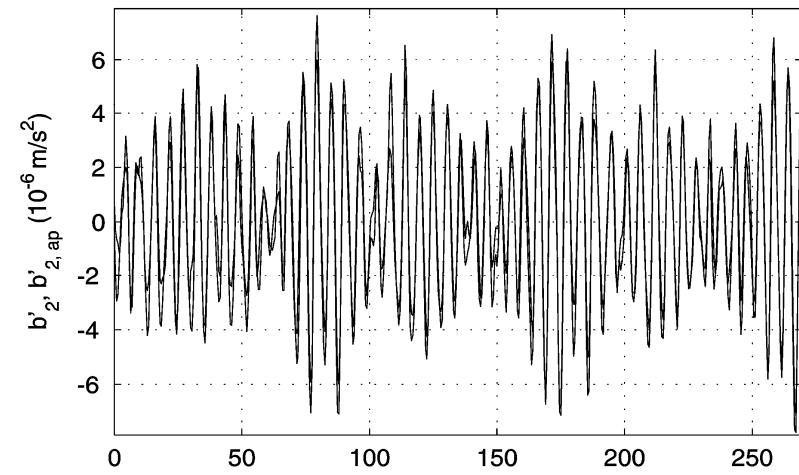


(b)

Fig. 4. The filtered acceleration component  $b'_1$  in interval 13; (a) the spectra, (b) the harmonic approximation and its error.

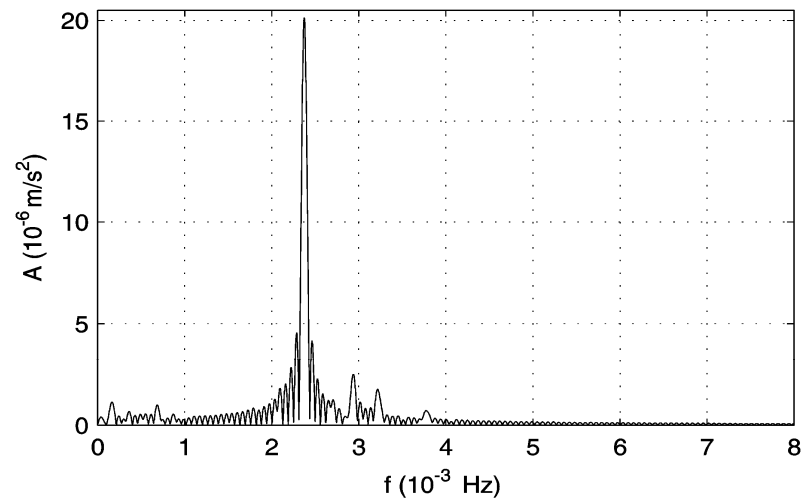
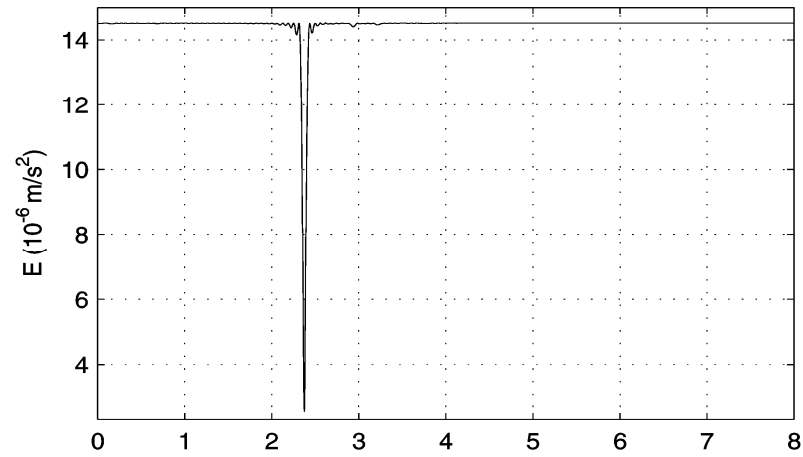


(a)

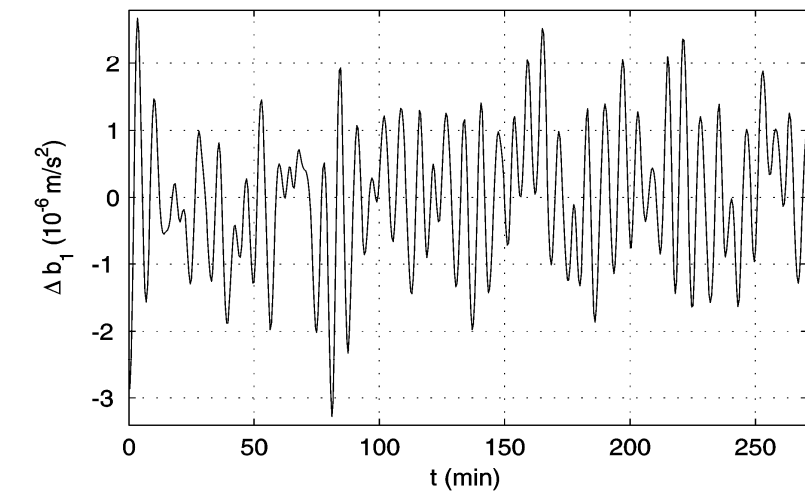
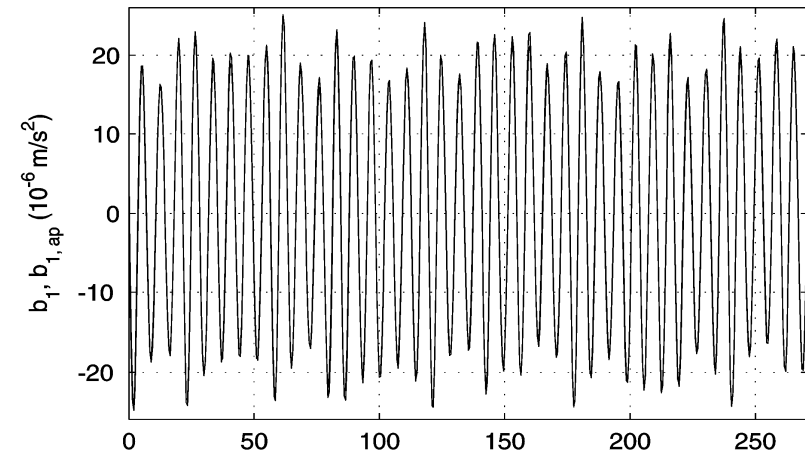


(b)

Fig. 5. The filtered acceleration component  $b'_2$  in interval 13; (a) the spectra, (b) the harmonic approximation and its error.

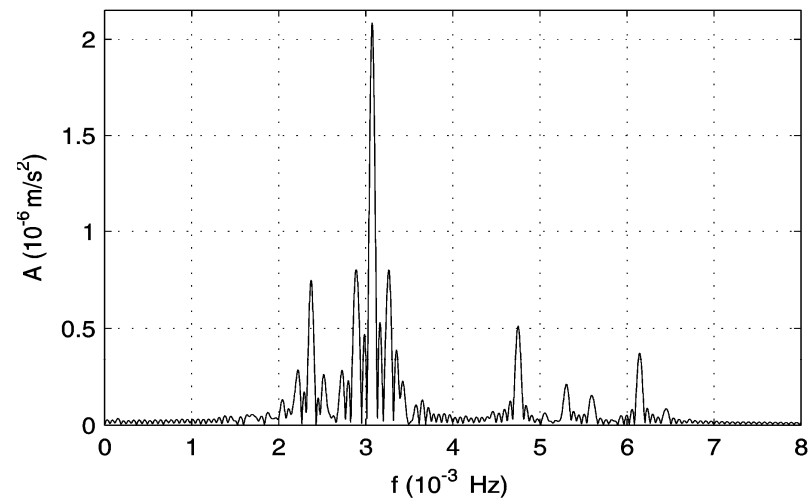
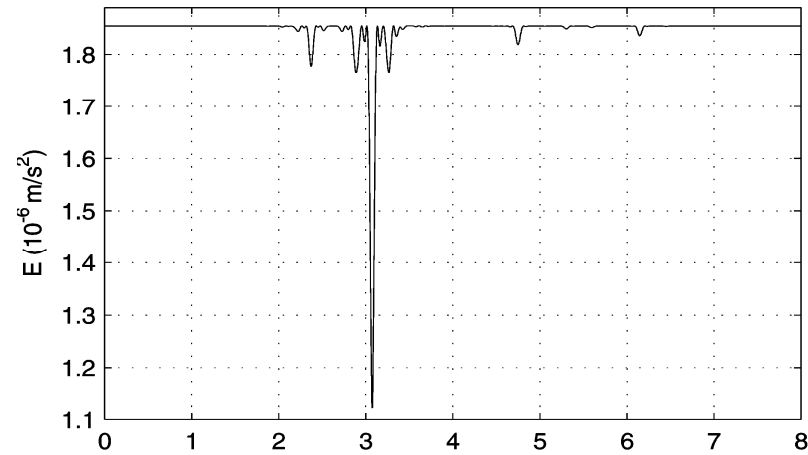


(a)

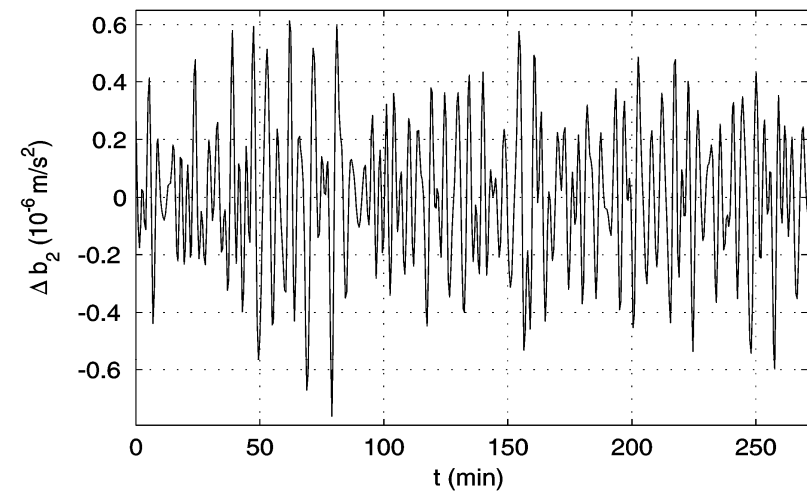
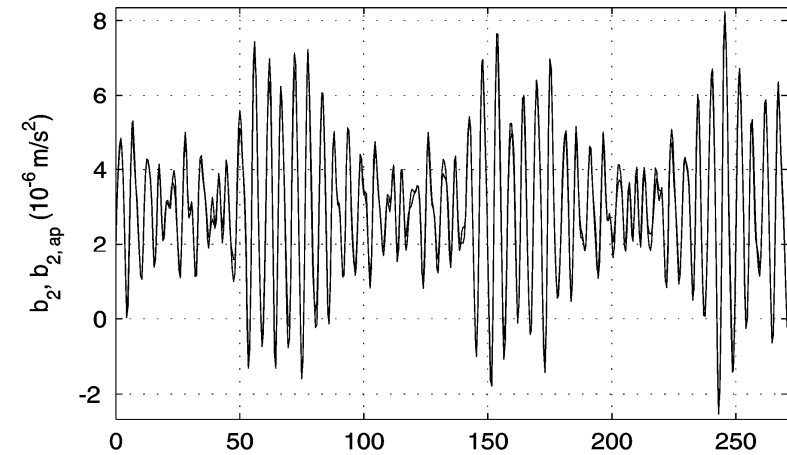


(b)

Fig. 6. The calculated acceleration component  $b_1$  in interval 13; (a) the spectra, (b) the harmonic approximation and its error.

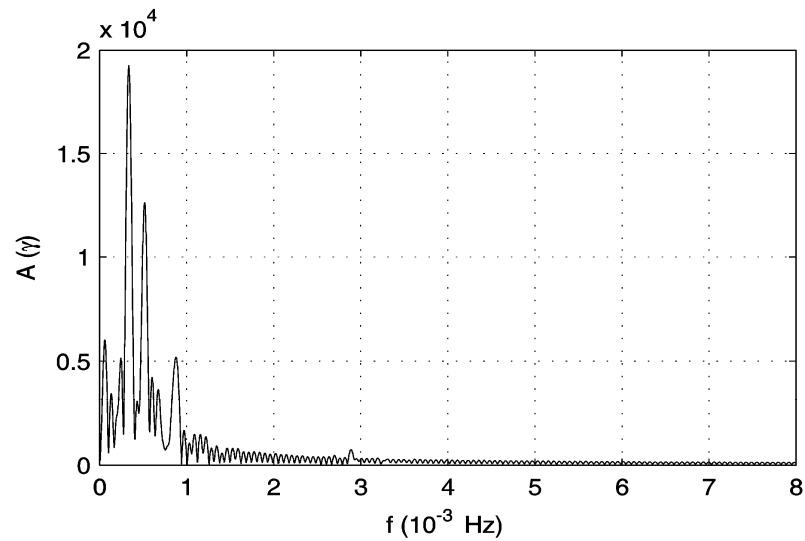
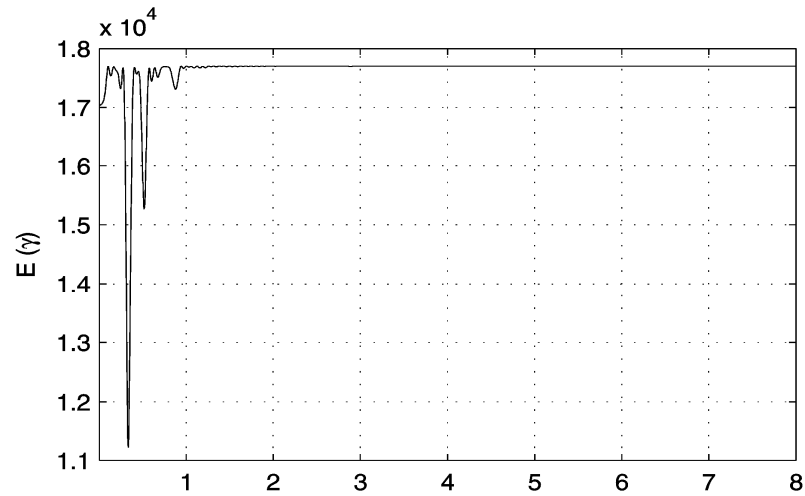


(a)

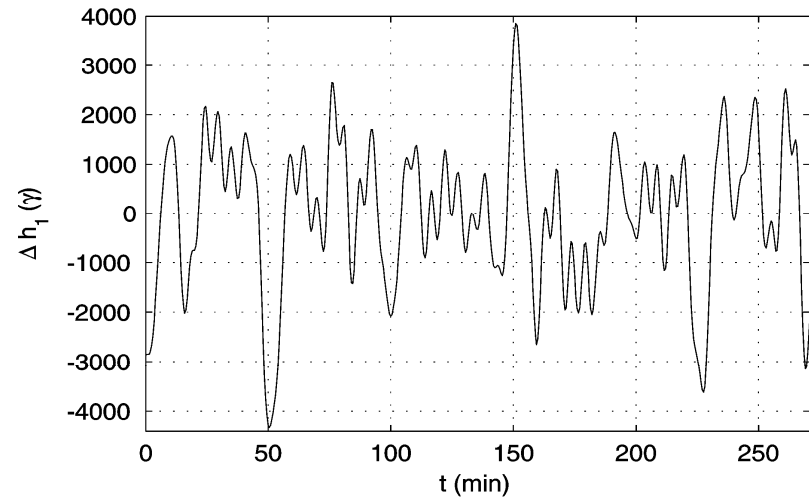
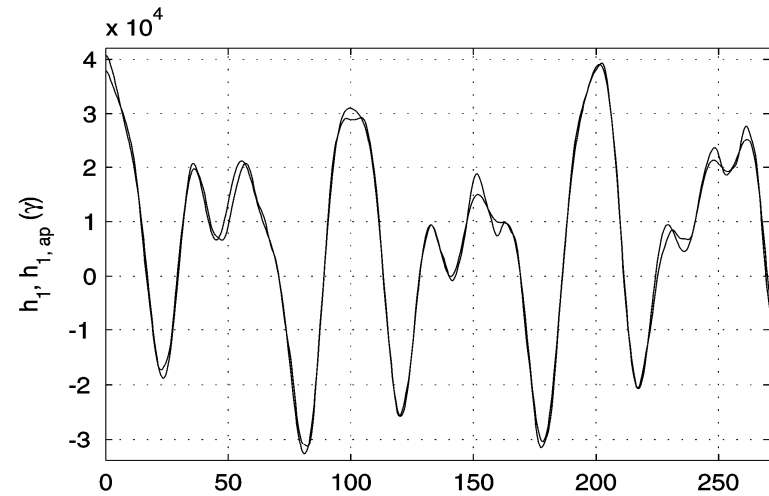


(b)

Fig. 7. The calculated acceleration component  $b_2$  in interval 13; (a) the spectra, (b) the harmonic approximation and its error.

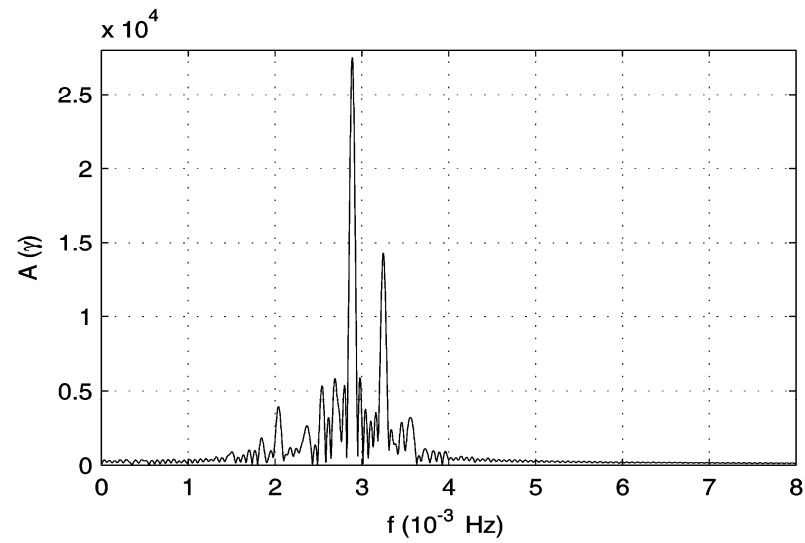
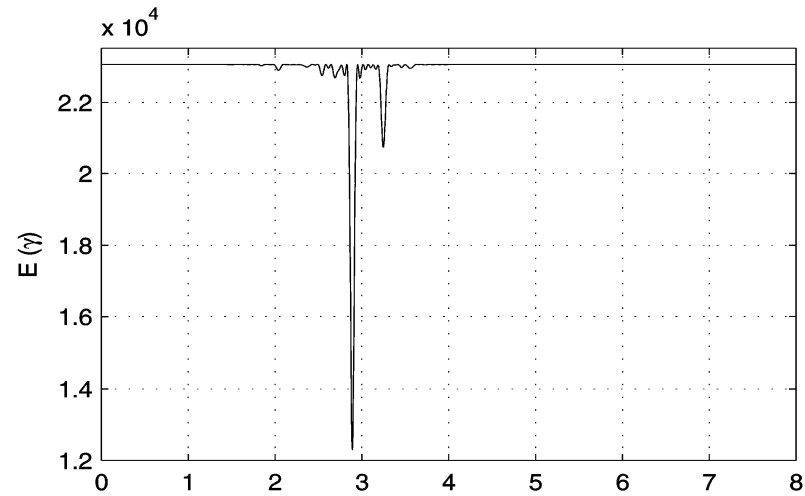


(a)

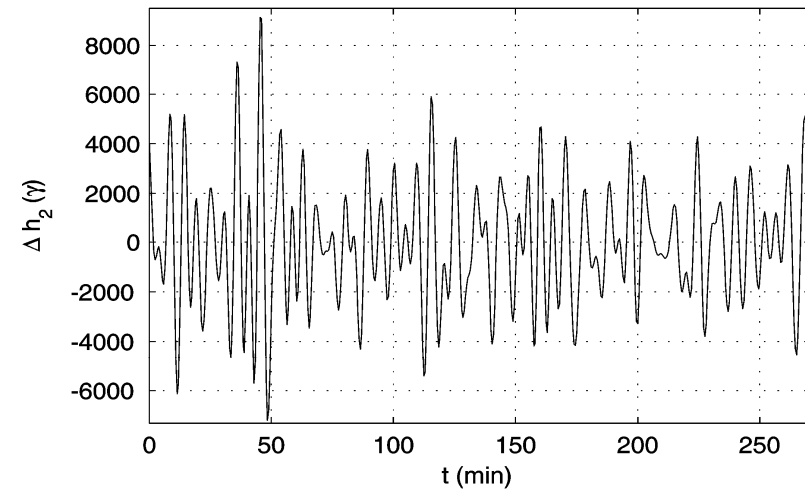
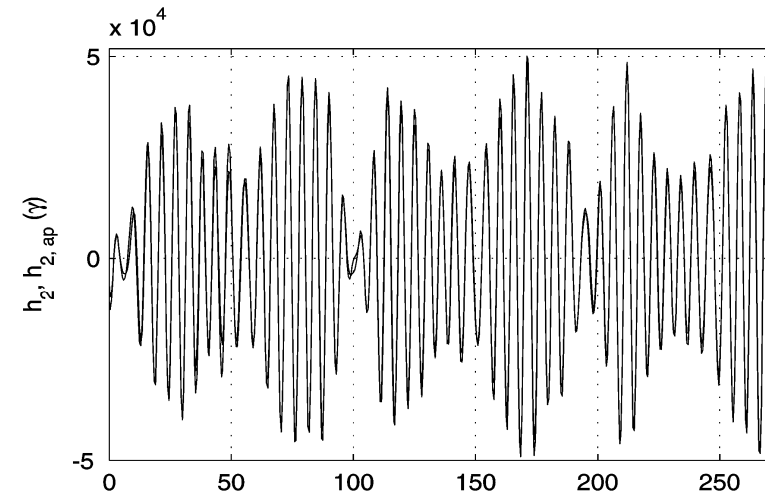


(b)

Fig. 8. The component  $h_1$  of calculated strength of the Earth magnetic field in interval 13;  
 (a) the spectra, (b) the harmonic approximation and its error.



(a)



(b)

Fig. 9. The component  $h_2$  of calculated strength of the Earth magnetic field in interval 13; (a) the spectra, (b) the harmonic approximation and its error.

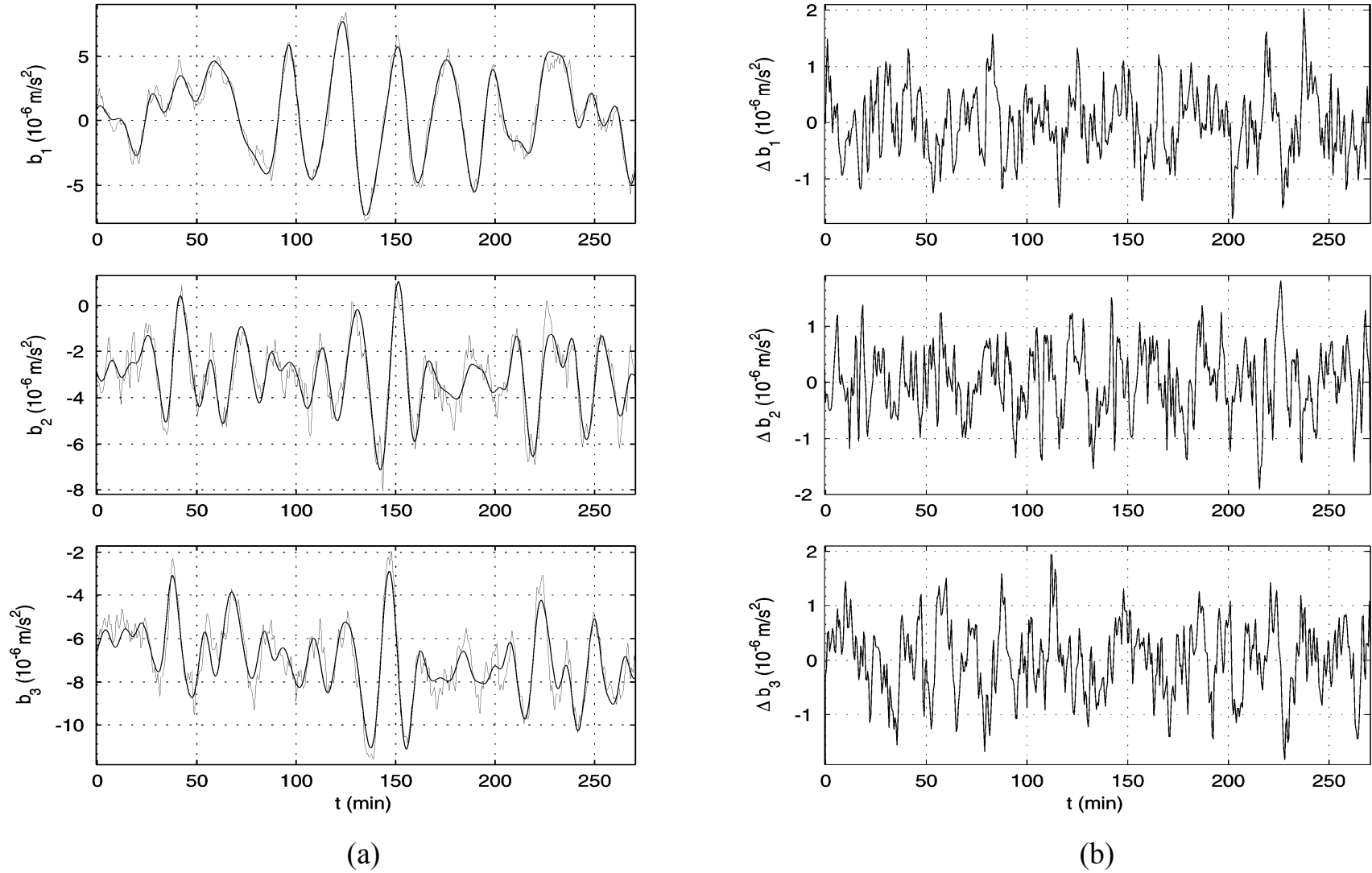


Fig. 10. The accelerations at the point of TAS3 location in interval 2,  $\sigma_b = 6.7 \cdot 10^{-7} \text{ m/s}^2$ ; (a) the corrected filtered functions  $\hat{b}_i(t)$  and their calculated analogs  $b_i(t)$ , (b) the differences  $\Delta b_i(t) = \hat{b}_i(t) - b_i(t)$

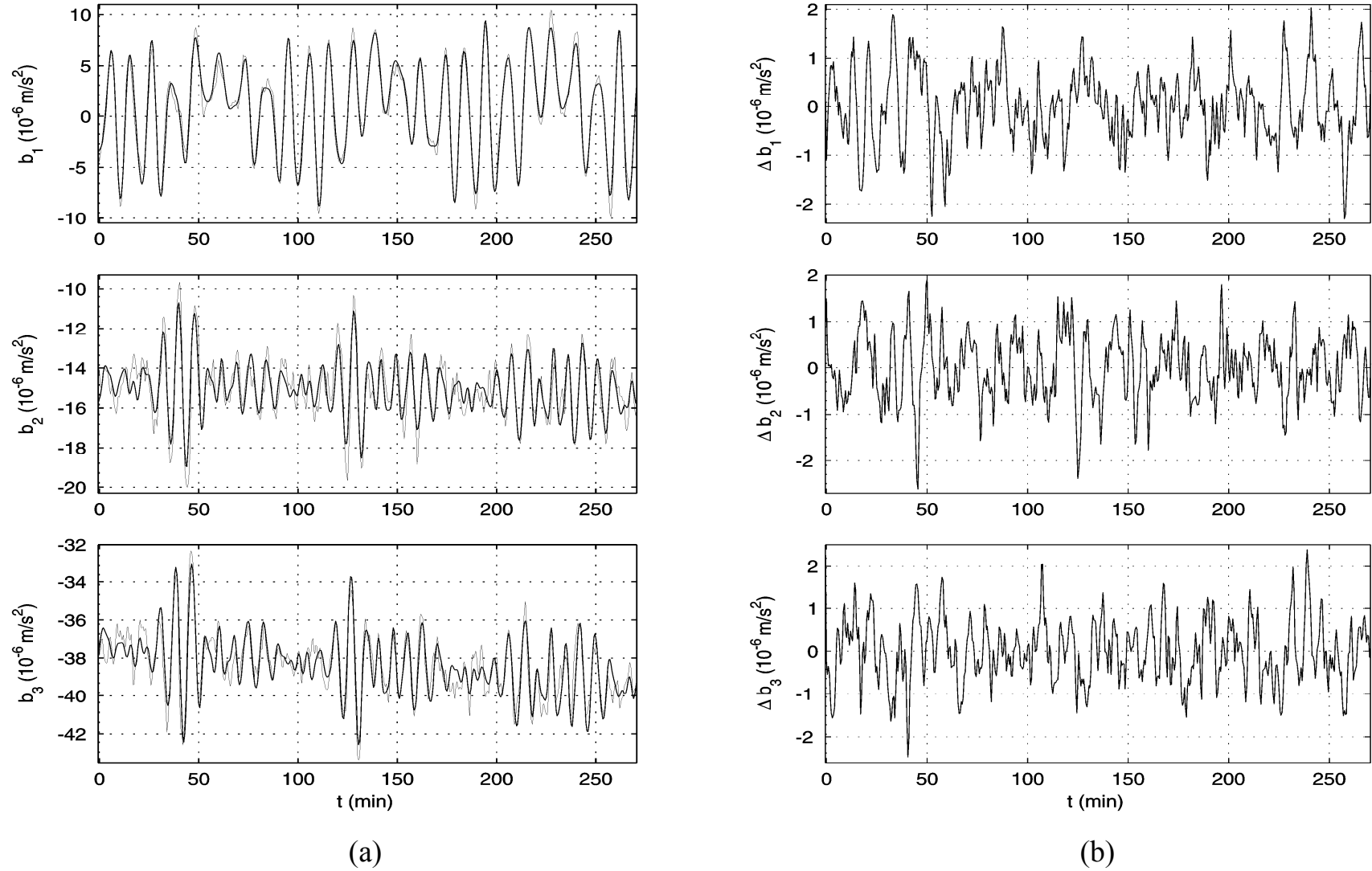


Fig. 11. The accelerations at the point of TAS3 location in interval 6,  $\sigma_b = 7.5 \cdot 10^{-7} \text{ m/s}^2$ ; (a) the corrected filtered functions  $\hat{b}_i(t)$  and their calculated analogs  $b_i(t)$ , (b) the differences  $\Delta b_i(t) = \hat{b}_i(t) - b_i(t)$ .

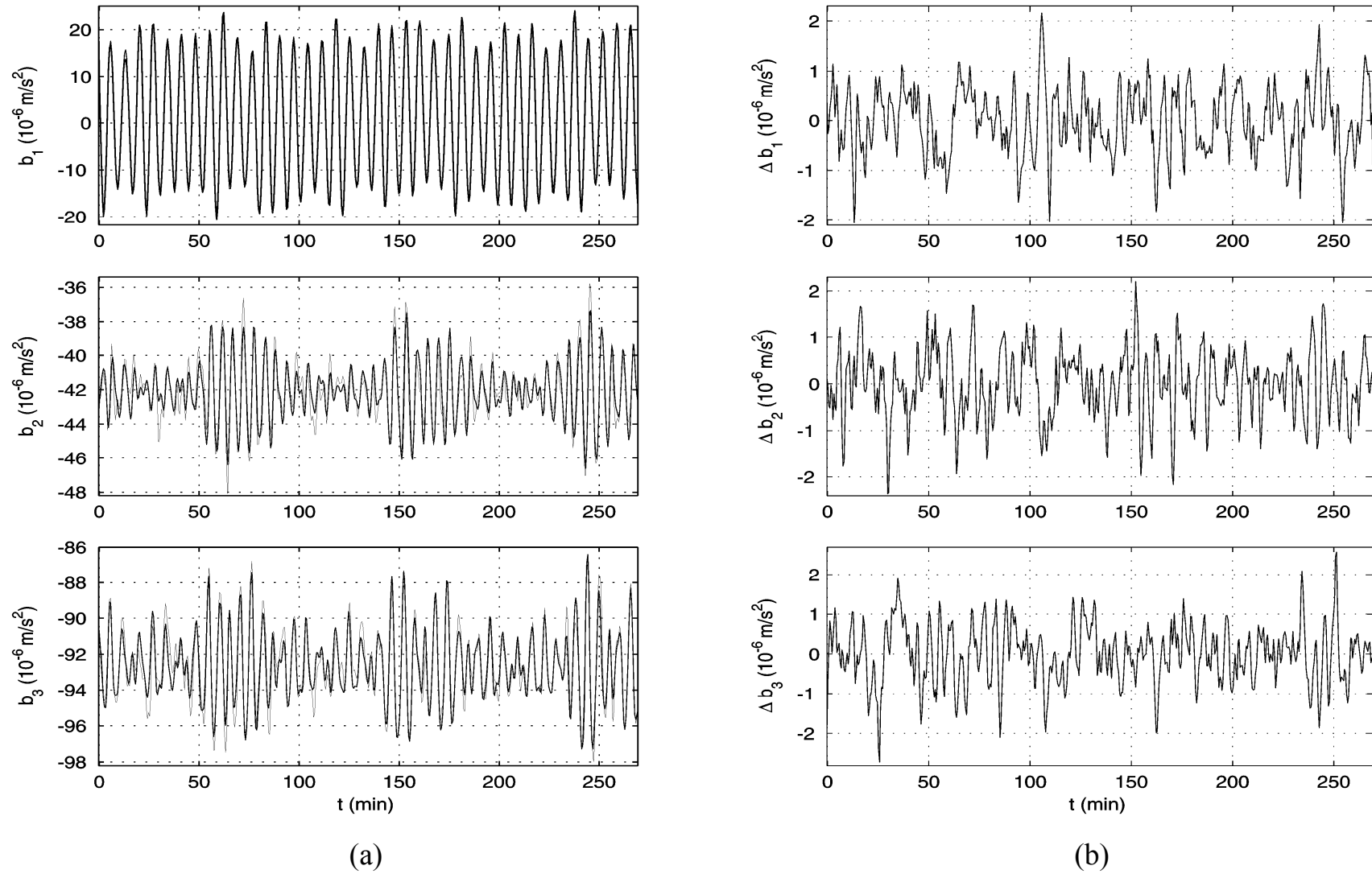


Fig. 12. The accelerations at the point of TAS3 location in interval 13,  $\sigma_b = 7.3 \cdot 10^{-7} \text{ m/s}^2$ ; (a) the corrected filtered functions  $\hat{b}_i(t)$  and their calculated analogs  $b_i(t)$ , (b) the differences  $\Delta b_i(t) = \hat{b}_i(t) - b_i(t)$ .